https://doi.org/10.5194/egusphere-2026-6446
Preprint. Discussion started: 16 November 2026
© Author(s) 2026. CC BY 4.0 License.

Ocean forcing of the Greenland Ice Sheet in the Ice Sheet Model Intercomparison Project 7 (ISMIP7)

Donald Slater[1], Lizz Ultee[2,3], Denis Felikson[4], Naveen Senthil[5], Heiko Goelzer[6], Michael Wood[7], Timothy C. Bartholomaus[8], M. Femke de Jong[9], and María-Paz Lira[6]

[1]School of Geosciences, University of Edinburgh, Edinburgh, UK
[2]NASA Goddard Space Flight Center, Greenbelt, MD, USA
[3]GESTAR-II Cooperative Agreement, Morgan State University, Baltimore, MD, USA
[4]NASA Goddard Space Flight Center, Greenbelt, MD, USA
[5]Department of Earth Sciences, University at Buffalo, Buffalo, NY, USA
[6]NORCE Research, Bjerknes Centre for Climate Research, Bergen, Norway
[7]Moss Landing Marine Laboratories, San José State University, Moss Landing, CA, USA
[8]Department of Earth and Spatial Sciences, University of Idaho, Moscow, ID, USA
[9]Department of Ocean Systems, Royal Netherlands Institute for Sea Research NIOZ, Texel, The Netherlands

Correspondence: Donald Slater (donald.slater@ed.ac.uk)

Abstract. Submarine melting and calving at ocean-terminating glaciers is a significant term in the mass budget of the Greenland Ice Sheet. Yet, accounting for these processes in sea level projections remains challenging due to evolving process understanding and the disparity in scale between the local detail needed and the coarse resolution of global models. Here, we present the protocol for ocean forcing of Greenland Ice Sheet models taking part in the Ice Sheet Model Intercomparison Project 7 (ISMIP7). We describe how earth system model output is bias-corrected and downscaled to obtain highly resolved fields of the two key variables needed to estimate submarine melt rate: subglacial discharge and ocean thermal forcing. These fields are provided for both historical and projection periods, and for a range of emissions scenarios. Ice sheet modelers are free to choose a parameterisation that converts these fields into estimated submarine melt. Similarly, the representation of calving is left up to the ice sheet modeler, subject to some recommendations. Aiming to facilitate evaluation of ice sheet models, we also provide our best estimate of how subglacial discharge and ocean thermal forcing have evolved in recent decades, but we highlight that this has significant uncertainty, particularly in the ocean. Relative to the previous iteration (ISMIP6), the protocol is less constraining, invokes submarine melt observations, and has improved ocean downscaling and bias correction. However, there remains significant room for improving treatment of the ice-ocean boundary in models; for example in the representation of calving, in the quantification of shelf mixing processes, and in greater use of ocean observations.

1 Introduction

Ice sheets are a leading factor in the global sea level budget both in the recent past and near future. Yet, limited understanding of key processes, difficulty representing and resolving these processes in models and uncertain boundary conditions all contribute to substantial spread in projections of future global sea level change arising from ice sheets (Goelzer et al., 2020;

https://doi.org/10.5194/egusphere-2026-6446
Preprint. Discussion started: 16 November 2026
© Author(s) 2026. CC BY 4.0 License.

Seroussi et al., 2020). Motivated by this problem, the Ice Sheet Model Intercomparison Project for CMIP7 (ISMIP7) seeks to provide community consensus estimates of the contribution of Antarctica and Greenland to sea level over the coming decades and centuries. ISMIP7 follows from its predecessor, ISMIP6, for which the overarching protocol was described in Nowicki et al. (2020), the ice sheet simulation results in Goelzer et al. (2020) for Greenland and Seroussi et al. (2020) for Antarctica, and the overall land ice results in Edwards et al. (2021). ISMIP7 is structured into several focus groups who together define the experimental protocol and provide the climate forcing files needed for ice sheet modelers in the community to run their simulations. This paper describes the proposed ISMIP7 protocol and files for forcing of the Greenland Ice Sheet by the ocean. The described protocol has also been adopted for the ice-sheet model experiments in the Tipping Points Modelling Intercomparison Project ("TIPMIP-ICE SHEETS"; Winkelmann/Klose et al., in prep.; Winkelmann et al., 2025), but the two efforts diverge in the climate experiments that they run. The present manuscript focuses on the ISMIP7 context.

The impact of the ocean on the Greenland Ice Sheet arises from myriad processes, including the large-scale ocean circulations that control ocean temperature in the basins surrounding the ice sheet (Straneo and Heimbach, 2013), continental shelf processes that allow access of offshore waters to fjords (Wood et al., 2021; Morrison et al., 2023), circulation within fjords (Mortensen et al., 2013; Straneo and Cenedese, 2015; Carroll et al., 2017), submarine melting of grounded glaciers and floating ice tongues (Wilson et al., 2017; Sutherland et al., 2019), and iceberg calving and all of its modulating factors such as melt undercutting and mélange buttressing (Benn et al., 2017; Fried et al., 2018; Rignot et al., 2015; Meng et al., 2025). Representing the impact of the ocean on the Greenland Ice Sheet to produce reliable projections of mass change is challenging due to multiple factors: (i) the relevant processes are complex and not understood sufficiently to consistently reproduce observations within models; (ii) the ice-ocean system is highly underconstrained by observations; and (iii) the large-scale models required to represent the ocean or ice sheet either do not or only partly resolve the relevant processes. However, an effort as large as ISMIP7, which relies on the volunteer contributions of modelers, requires that some guidance be offered for how a modeler can credibly and efficiently include poorly understood processes. Furthermore, the protocol must be accessible to ice sheet models with various degrees of complexity. For these reasons, the protocol must be sufficiently simple to implement in numerical models with spatial and temporal resolution far coarser than the processes it seeks to represent while also striving to stay true to the best present understanding of the processes.

The protocol for ocean forcing of the Greenland Ice Sheet in ISMIP6 contained two possible ocean forcing implementations (Slater et al., 2020). The first, called the "retreat implementation," was a precomputed time-variable ice mask imposed on the ice sheet model. The second, called the "submarine melt implementation," prescribed an estimated melt rate at the ice-ocean boundary. Models using the submarine melt implementation generally gave slightly smaller sea level contributions by 2100 (Goelzer et al., 2020).

Under the retreat implementation, advance or retreat of marine-terminating glaciers was linearly related to change in submarine melt rate, which was in turn estimated using subglacial discharge and ocean thermal forcing derived from global climate (Coupled Model Intercomparison Project, "CMIP") models. The retreat implementation had the advantages of being empirically calibrated to observations from recent decades (Slater et al., 2019), of being easily implementable across many models, was consistent with the consensus that submarine melt is an important driver of glacier retreat (e.g., Wood et al., 2021) and

https://doi.org/10.5194/egusphere-2026-6446
Preprint. Discussion started: 16 November 2026
© Author(s) 2026. CC BY 4.0 License.

had a single parameter to test sensitivity to. It also had significant downsides, notably that the regression of terminus position versus submarine melt on which the parameterisation was built was relatively weak, and the highly constraining nature of the approach took the ice dynamic feedback on terminus position (e.g., Catania et al., 2020) away from the ice sheet model and into the retreat parameterisation. Relatedly, its form ensured that if the climate stabilised then the glacier terminus position was immediately fixed, which contravenes the observation that glaciers take time to equilibrate with climate (Robel et al., 2018). The disconnection of terminus position from ice dynamics also becomes more problematic the longer one wishes to simulate; for example, out to 2300.

The submarine melt implementation was far less constraining, allowing an ice sheet model to resolve the balance at the front of a glacier between terminus position change, ice velocity, calving and submarine melting (e.g., Bondzio et al., 2016; Morlighem et al., 2016; Todd et al., 2018). This restores the role of ice dynamics in terminus position change to the ice sheet model and allowed models with relatively mature calving routines to take advantage of their abilities. On the other hand, relatively few models were able to implement this approach in ISMIP6, there are very few observations of submarine melt rate to constrain the parameterisation, and the science is far from settled on how best to represent calving in continental-scale ice sheet models.

Both implementations had significant simplifications with respect to ocean and fjord processes. The retreat implementation employed regional ocean temperatures averaged over seven ocean sectors with no consideration of fjord processes, while the submarine melt implementation used the same regional averaging but did account for the potential for bathymetric blocking of dense waters. Neither implementation accounted for processes beyond submarine melt that affect calving (in particular, ice mélange), and, by providing only annual forcing, neither implementation accounted for seasonality.

The Greenland ocean forcing protocol for ISMIP7, described below, builds on these reflections and lessons from ISMIP6. This paper proceeds as follows: section 2 provides a high-level overview of the proposed protocol; section 3 describes in detail the required processing of climate model output; section 4 addresses how the climate forcing should be used to estimate submarine melt and calving fluxes; section 5 provides example forcings based on the climate model CESM2-WACCM; then we finish with discussion and conclusions. Technical details, such as dataset formatting, are provided in Appendix B.

2 Overview of ISMIP7 Greenland ocean forcing

The proposed datasets and protocol can be used to estimate submarine melt rate at the marine margin of the ice sheet (Fig. 1), for a given climate scenario in a CMIP simulation. The protocol is ultimately similar to the ISMIP6 submarine melt implementation (Nowicki et al., 2020; Slater et al., 2020), but with improved temporal resolution of the forcing datasets, improved extrapolation of ocean properties into fjords, improved bias correction and a relaxation of the protocol in a few areas. The protocol does not include the retreat implementation, as had been part of ISMIP6.

For grounded marine-terminating glaciers, having approximately vertical calving fronts, submarine melting acts horizontally into the calving front (Fig. 1a). In a flowline sense and in a time interval δt, the movement of the calving front, δl, is given by

$$\delta l = v\,\delta t - c\,\delta t - m\,\delta t \tag{1}$$

https://doi.org/10.5194/egusphere-2026-6446
Preprint. Discussion started: 16 November 2026
© Author(s) 2026. CC BY 4.0 License.

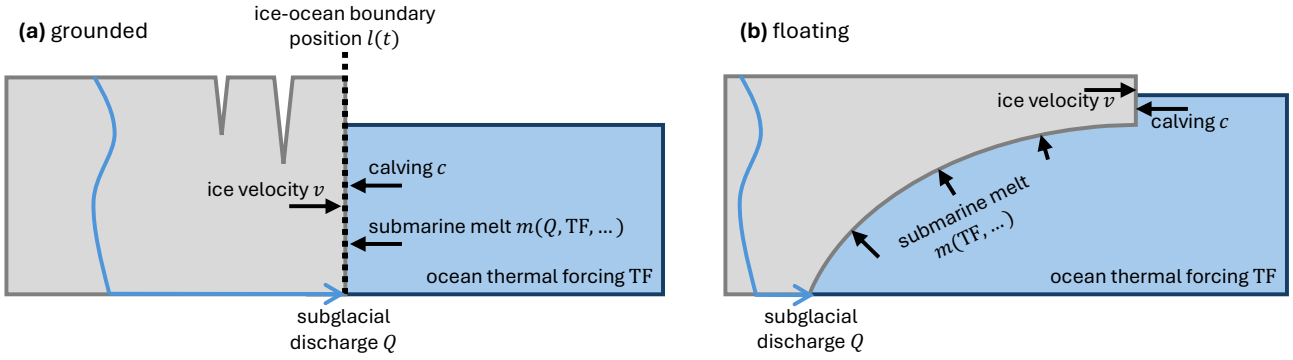


Figure 1. Schematics illustrating the physical system for (a) grounded marine-terminating glaciers and (b) floating ice tongues. Our protocol provides files specifying the subglacial discharge and ocean thermal forcing in both cases. The use of these variables to estimate submarine melt rate and to treat calving is left to the ice sheet model.

Where v is the frontal ice velocity, $c\delta t$ is the length lost to calving (or if conceptualising calving as a rate, c is the calving rate) and m is the submarine melt rate (Fig. 1a). The total loss from the glacier, $c\delta t + m\delta t$, is the frontal ablation (or $c + m$ is the frontal ablation rate). Submarine melting at grounded marine-terminating glaciers is known to depend principally on the subglacial discharge (Motyka et al., 2013; Jackson et al., 2022) and the ocean thermal forcing (Luckman et al., 2015) and it is these two factors that we provide as datasets to estimate submarine melt rate. Choice of the submarine melt parameterisation, treatment of calving, and the overall resulting movement of calving fronts, is left to the ice sheet modeler, however guidance is provided in sections 4.1 & 4.2 below. Clearly, within an ice sheet model, the conversion of these conceptual linear quantities to volumes requires multiplication by width and depth.

At floating ice tongues/shelves, submarine melting instead acts approximately vertically into the approximately horizontal ice-ocean interface (Fig. 1b; the protocol does not consider submarine melting of the vertical ice shelf calving front). In this case, submarine melt would enter the continuity equation in the ice sheet model. We again provide datasets of subglacial discharge and ocean thermal forcing that can be used to estimate submarine melt rate, but the melt parameterisation and treatment of the calving front is left to the ice sheet modeler.

The principal datasets of subglacial discharge and ocean thermal forcing are derived from CMIP Atmosphere-Ocean General Circulation Model (AOGCM) output for a given climate scenario using the process illustrated in Fig. 2. Subglacial discharge is derived by the following steps: (i) downscaling of CMIP AOGCM atmospheric variables to estimate ice sheet surface runoff; (ii) summing of surface runoff over glacier drainage basins; and (iii) bias-correction against RACMO2.3p2 output (Noël et al., 2018). Ocean thermal forcing is derived by (i) calculating ocean thermal forcing in the CMIP AOGCM; (ii) regridding to a regularly-spaced grid; (iii) bias-correction against EN4.2.2 output (Good et al., 2013); and (iv) extrapolation from the continental shelf into fjords.The bias-correction period is 1985-2014 and the final datasets are provided at 1-km spatial resolution, monthly, over the full period of the CMIP simulation (which varies by simulation and starts as early as 1850 and ends as late as 2300).

https://doi.org/10.5194/egusphere-2026-6446
Preprint. Discussion started: 16 November 2026
© Author(s) 2026. CC BY 4.0 License.

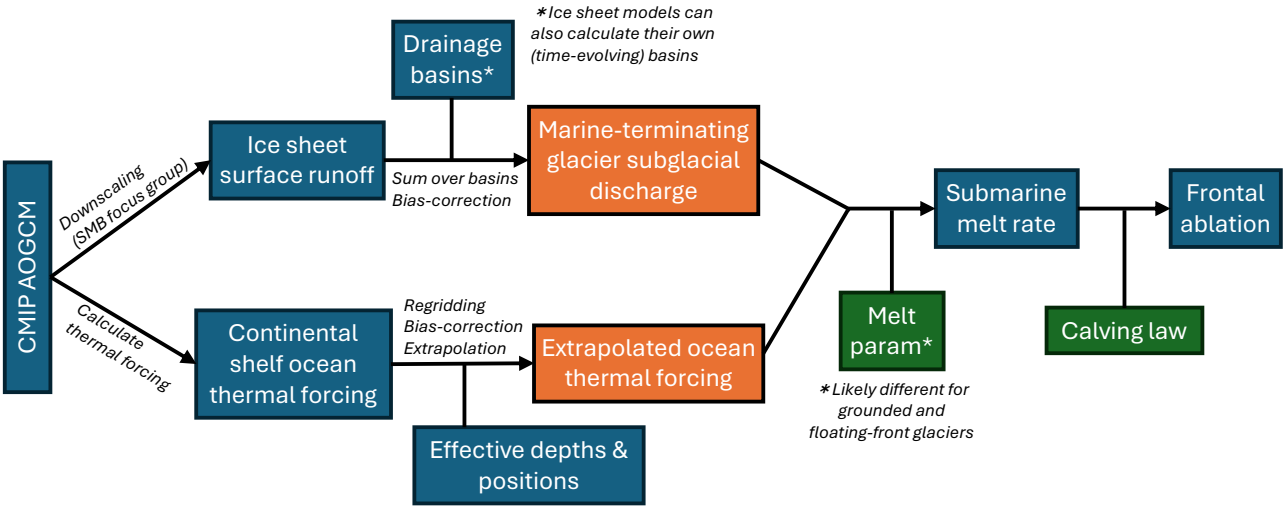


Figure 2. Flowchart of the protocol and processing, starting from CMIP AOGCM output and ending with frontal ablation implemented in an ice sheet model. Orange backgrounds indicate the main forcing files supplied for ice sheet modelers (though ice sheet surface runoff is available for modelers who wish to use their own drainage basins). Green backgrounds indicate choices that need to be made by ice sheet modelers.

We also produce forcing datasets for an "observationally-constrained experiment" (OCX). This is intended to be our "best estimate" of how subglacial discharge and ocean thermal forcing have evolved in recent decades (as well as being biased in the mean, CMIP AOGCMs are unlikely to have the same trends and interannual variability as has been observed in recent decades). We create the OCX forcing directly from RACMO-estimated subglacial discharge and EN4-estimated ocean thermal forcing. The procedure is the same as for a CMIP AOGCM (Fig. 2), but there is no bias correction step. The OCX forcing spans 1958-2025 at the same spatial and temporal resolution as the other datasets.

3 Processing of CMIP AOGCM output

3.1 Subglacial discharge

The objective is to provide a gridded subglacial discharge field such that wherever an ice sheet model has a marine-terminating glacier terminus (i.e., an ice-ocean boundary pixel where the bed is below sea level), the field can be sampled at that location to obtain an estimate of the total subglacial discharge for that glacier/basin. This is achieved as follows.

3.1.1 Ice sheet surface runoff

Ice sheet surface runoff is obtained from the CMIP AOGCM. ISMIP7 has chosen two core AOGCMs: CESM2-WACCM (Danabasoglu et al., 2020) and MRI-ESM2-0 (Yukimoto et al., 2019). For the former, runoff is obtained by direct statistical

https://doi.org/10.5194/egusphere-2026-6446
Preprint. Discussion started: 16 November 2026
© Author(s) 2026. CC BY 4.0 License.

downscaling of runoff output by CESM2-WACCM. Specifically, for each month, the CMIP AOGCM output (with a resolution on the order of 100 km) is used to form a spatially-local linear relationship between runoff and ice sheet surface elevation. This linear relationship is then used to estimate surface runoff at 1-km resolution for each month, given ice sheet surface elevation at the same resolution. Note that this method assumes static ice sheet surface elevation, but that the surface mass balance-elevation feedback is accounted for in the surface mass balance applied by the ice sheet models (Nowicki et al., in prep). For MRI-ESM2-0, the lack of a snow module meant that it was necessary to run the surface energy balance model GEMB (Gardner et al., 2023) before downscaling. Further details are in the overall ISMIP7 protocol paper (Nowicki et al., in prep).

3.1.2 Drainage basins

The next step is to define the subglacial hydrological drainage basins. This is typically done using flow routing on the hydrological potential, which depends on both the bed topography and the ice thickness (Shreve, 1972). However, such an approach often produces several drainage basins draining through each outlet glacier (e.g., Mankoff et al., 2020). Since ice sheet models are generally not at the stage of dealing with multiple drainage outlets at a single calving front, the associated drainage basins have to be combined to obtain a single drainage basin for each outlet glacier, a process which is manual, labour intensive and difficult to reproduce. Here, we take a different approach which is to use the pre-defined drainage basins of Mouginot and Rignot (2019) (Fig. 3a). Note that we only consider the basins that are part of the main ice sheet, therefore excluding disconnected glaciers and ice caps. It is important to note that these basins are ice drainage basins; that is, they are based on ice flow rather than subglacial water flow. However in practice, the differences between ice and hydrological basins are minor, especially once we sum the runoff over the basins to obtain subglacial discharge. The benefit of using these ice drainage basins is a significant saving in manual processing and a more reproducible workflow.

For some period of time in some ice sheet models, it is possible that the simulated ice sheet will extend beyond the present-day basins, and to accommodate these simulations we need to have estimated subglacial discharge beyond the basins. To do this, each pixel that is not presently within the ice sheet but is close to the ice sheet (as defined by a convex hull boundary - see section 3.2.2) is assigned to the nearest basin (Fig. 3b). Pixels that are beyond the convex hull are not assigned a basin but are assigned a nominal subglacial discharge (section 3.1.3). The intention is to allow simulations where the ice extent is slightly larger than expected to use the present-day basins. Simulations where the ice extent is much larger than expected can still apply this protocol and run without crashing but do not use the present-day basins as these likely make less sense if the ice extent was much larger.

A weakness of this approach is that it uses drainage basins that are fixed in time. In reality, particularly out to 2300, the ice sheet geometry will evolve and may change the drainage basins. Some ice sheet models may therefore prefer to dynamically calculate their own drainage basins; we allow for this within the protocol (Fig. 2) and make the surface runoff fields available so that ice sheet modelers can calculate the subglacial discharge consistent with their basins.

https://doi.org/10.5194/egusphere-2026-6446
Preprint. Discussion started: 16 November 2026
© Author(s) 2026. CC BY 4.0 License.

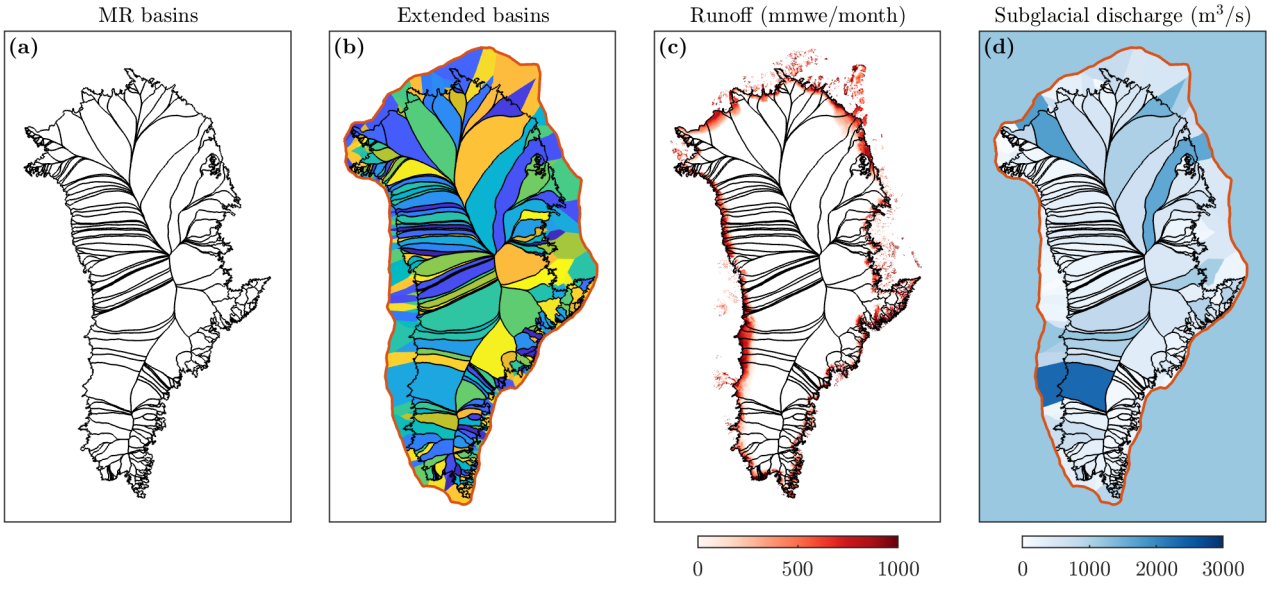


Figure 3. Process to obtain subglacial discharge. (a) drainage basins, excluding those that are not part of the main ice sheet. (b) Extended basins; shading indicates pixels lying in the same basin. (c) Example of spatial runoff field, in this case for July 2024 from RACMO. (d) Basin subglacial discharge, obtained by summing the runoff field over the drainage basins. Note that we only sum runoff from the main ice sheet.

3.1.3 Aggregation and bias-correction

To obtain the estimated basin subglacial discharge, we sum the surface runoff field (e.g., Fig. 3c) over the original basins (Fig. 3a) and assign the resulting value to all pixels in the extended basin (Fig. 3d). Note that we sum the runoff over the original basins, rather than the extended basins, to exclude runoff from disconnected ice caps that should not contribute to subglacial discharge from the main ice sheet. Beyond the extended basins, we assign a spatially-constant subglacial discharge equal to the total ice sheet-wide discharge divided by 50; the motivation being that an ice sheet extended to the continental shelf might have 50 large ice streams. We anticipate that no simulation will end up using this value but include it as an appropriate order-of-magnitude estimate just in case.

The last step to providing estimated subglacial discharge is the bias correction. Since CMIP AOGCMs can have large temperature biases in the Greenland region (Barthel et al., 2020), the estimated subglacial discharge can be much larger or smaller than our best estimate over recent decades. To bring the CMIP AOGCMs into line with our best estimates, we therefore subtract a constant monthly offset from the full time series, which is the mean difference in that month between the RACMO2.3p2 (Noël et al., 2018) and CMIP AOGCM subglacial discharge over the 1985-2014 time period. For winter months this can result in a few slightly negative subglacial discharge values that are subsequently set to 0.

https://doi.org/10.5194/egusphere-2026-6446
Preprint. Discussion started: 16 November 2026
© Author(s) 2026. CC BY 4.0 License.

3.2 Ocean thermal forcing process

The objective in defining ocean thermal forcing for ice sheet models is a form of "downscaling" that goes from the coarse (0.25–1 degree, or ∼100 km) resolution, irregularly-gridded CMIP ocean model output, to a field of grounding line ocean thermal forcing at any potential marine margin position, defined on the regular 1 km resolution ISMIP grid. The marine margin may be located within fjords that are not resolved by the CMIP model, or if there is significant ice loss then the margin may be located far inland of the present-day margin.

3.2.1 CMIP properties and bias correction

We first calculate thermal forcing in the CMIP model and bias-correct it to our best estimate of observed thermal forcing over recent decades, which we take to be the EN4 objective analysis v4.2.2 (Good et al., 2013). EN4 is an observationally-based estimate of ocean properties obtained by spatial and temporal interpolation of ocean profiles.

Thermal forcing, which is the difference between the in-situ temperature and freezing point, is calculated in both the AOGCM and EN4 as

$$\mathrm{TF}(i,z,t) = T(i,z,t) - [\lambda_1 S(i,z,t) + \lambda_2 + \lambda_3 z] \quad (2)$$

Where $T/S(i,z,t)$ are the temperature/salinity at grid point i, depth z (negative below the surface) and time t, while $\lambda_1 = -5.73\times10^{-2}\,^\circ$C/(g/kg) , $\lambda_2 = 8.32\times10^{-2}\,^\circ$C and $\lambda_3 = 7.61\times10^{-4}\,^\circ$C/m. Note that we use a linear spatial index i here rather than grid coordinates to emphasize that CMIP grids are often irregular (e.g., Fig. 4a).

The thermal forcing in CMIP and EN4 are then brought onto a common, regular vertical grid with resolution of 50 m, then a common, regular horizontal grid with resolution of 40 km, in both cases using linear interpolation and ensuring that we retain no data values at depths or locations where properties are undefined on the original grids (Fig. 4b).

The CMIP thermal forcing is then bias-corrected by quantile delta mapping (QDM), following Cannon et al. (2015) and Verjans et al. (2023). The QDM method adjusts the cumulative distribution function of the CMIP thermal forcing, both historical and projected, to match the cumulative distribution function of the EN4 dataset over the reference period (1985-2014) while allowing for change in the CDF over time. We apply this correction annually, thus correcting interannual variability while maintaining the seasonal variability simulated by the CMIP model. We remove the mean and the linear trend of both datasets, correct the cumulative distribution function of the residual in the CMIP data, and then impose the mean of the EN4 data and the trend of the CMIP data. The bias-corrected thermal forcing is thus

$$\mathrm{TF}_{\mathrm{corrected}}(x_{\mathrm{reg}},y_{\mathrm{reg}},z_{\mathrm{reg}},t) = \overline{TF}_{\mathrm{EN4}}(x_{\mathrm{reg}},y_{\mathrm{reg}},z_{\mathrm{reg}}) + \mathrm{TF}'_{\mathrm{CMIP}}(x_{\mathrm{reg}},y_{\mathrm{reg}},z_{\mathrm{reg}},t) + \widetilde{\mathrm{TF}}(x_{\mathrm{reg}},y_{\mathrm{reg}},z_{\mathrm{reg}},t) + \delta(x_{\mathrm{reg}},y_{\mathrm{reg}},z_{\mathrm{reg}},t) \quad (3)$$

Where $\overline{\mathrm{TF}}$ is the mean of EN4 data over the reference period, TF' is the linear trend in the CMIP data, $\widetilde{TF}$ is the QDM-corrected interannual variability, and δ is the residual monthly variability in the CMIP data. The bias-corrected TF is defined at every point and depth level of the common regular grid, maintaining no-data values where either the CMIP or EN4 data are undefined (Fig. 4c).

https://doi.org/10.5194/egusphere-2026-6446
Preprint. Discussion started: 16 November 2026
© Author(s) 2026. CC BY 4.0 License.

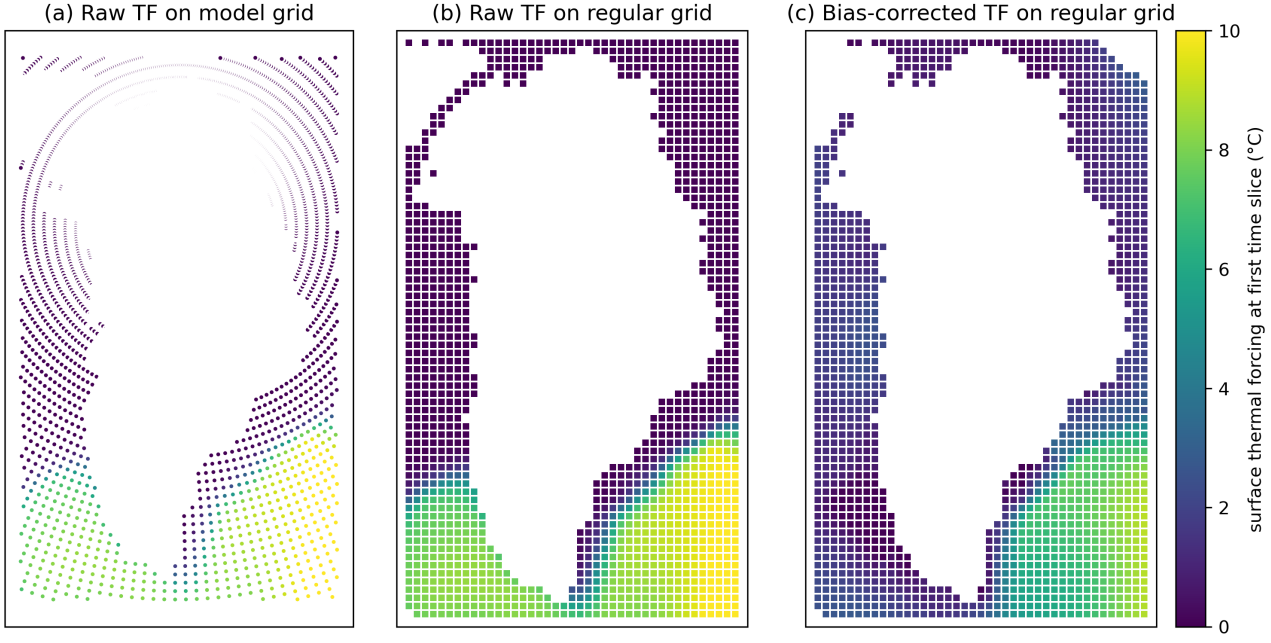


Figure 4. Illustration of thermal forcing processing steps applied to the first time slice (January 1850) of the CESM2-WACCM historical simulation. (a) Thermal forcing at the ocean surface calculated on the raw model grid. (b) Thermal forcing regridded to the regular horizontal and vertical grid used for bias correction. (c) Thermal forcing with bias correction applied (i.e., $TF_{corrected}$ from Eq. 3).

3.2.2 Effective depths and positions

The bias-corrected ocean properties so far (Fig. 4c) are defined offshore but not within Greenland's fjords. The first step in the extrapolation of properties into fjords is to obtain an effective depth $z_{\text{eff}}(x, y)$ for each below sea-level location (x, y) on the ISMIP grid; note that points on the 40-km resolution regular grid are denoted $(x_{\text{reg}}, y_{\text{reg}})$ while points on the 1-km resolution ISMIP grid are denoted (x, y). We define the effective depth as the greatest depth at which there is a continuous connection to an ocean basin with a depth exceeding 2000 m. To give an example, a location inside a fjord with a sill at 100 m depth will have an effective depth of 100 m, provided there is a path deeper than 100 m from the sill to the edge of the continental shelf. The effective depth is essentially the greatest depth at which a given below sea-level location is well connected to an ocean basin, a definition similar to previous studies (e.g., Morlighem et al., 2019; Slater and Straneo, 2022). We calculate the effective depth using BedMachinev5 bed topography (Morlighem, 2022) augmented by General Bathymetric Chart of the Oceans bathymetry (GEBCO, 2025) at the edges of the domain, with both products interpolated onto the 1-km ISMIP grid (Fig. 5a). The resulting effective depth is shown in Fig. 5b; effective depths on the continental shelf become more homogeneous than the original bathymetry while effective depths in the fjords and below the present-day ice sheet are influenced by sill and continental shelf depths. For example, many points in the Sermeq Kujalleq in Kangia (Jakobshavn Isbrae) ice catchment have an effective depth

https://doi.org/10.5194/egusphere-2026-6446
Preprint. Discussion started: 16 November 2026
© Author(s) 2026. CC BY 4.0 License.

of 250 m as this is the maximum sill depth at the mouth of Ilulissat Icefjord and the sill is the shallowest bathymetry between the ice catchment and the deep basin of Baffin Bay.

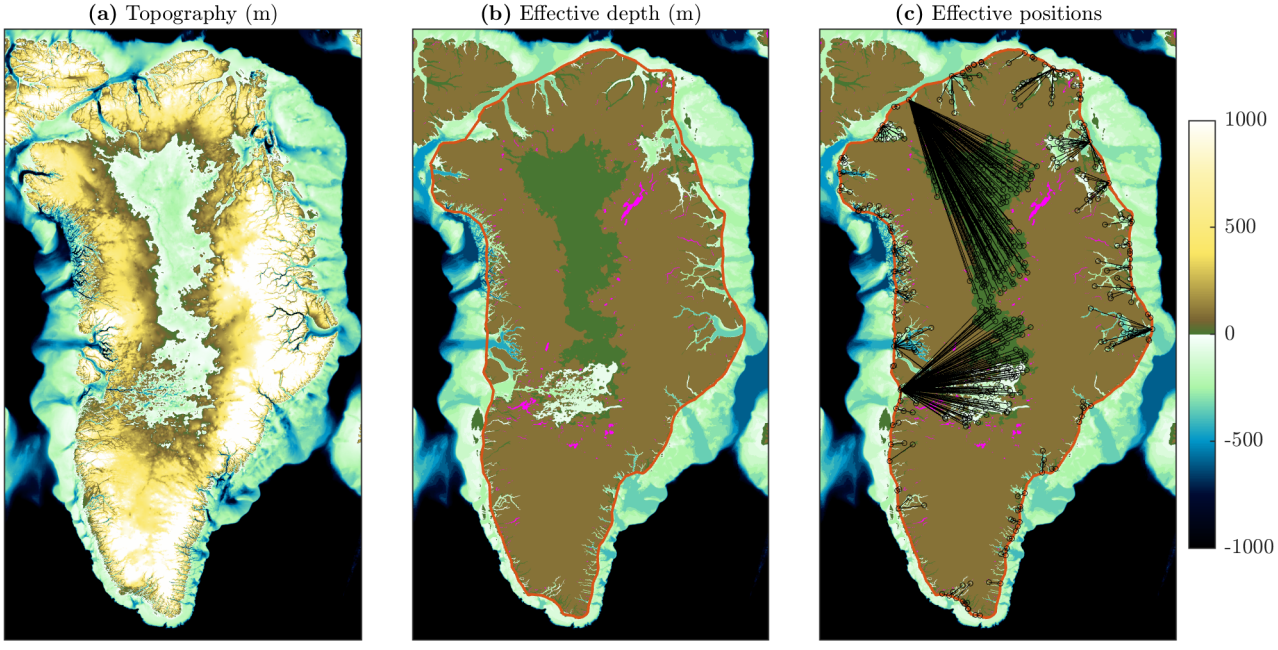


Figure 5. Illustration of effective depth and position. (a) 1-km resolution bed topography used for the calculation. (b) Effective depth, i.e., the deepest pathway from a below sea-level point to the deep ocean. The dark green area has an effective depth of 0 m; that is, it is connected to the ocean but only by a very shallow pathway. Magenta areas are below sea-level but are disconnected from the ocean. The red outline denotes the "convex hull" described in the text. (c) Effective positions for selected points inside the convex hull; the black lines link the points to their respective effective position.

The second step defines a "convex hull" for Greenland (Fig. 5b; red boundary). This is rather like stretching a rubber band around Greenland and then letting it contract onto the land. We use this to separate the domain into a region outside the convex hull (which is generally resolved by CMIP models) and a region inside the convex hull (which is almost exclusively not resolved).

In the third step, we define an effective position $[x_{\text{eff}}(x,y), y_{\text{eff}}(x,y)]$ for each below sea-level location $[x,y]$. The idea is that the effective position will provide the source waters that will ultimately make it to the location $[x,y]$. For locations outside the convex hull, the effective position is taken to be the same as the location itself $[x_{\text{eff}} = x, y_{\text{eff}} = y]$, because ocean properties at that point are likely to come from a CMIP model point close to that location. For points inside the convex hull, the effective position is the nearest point outside the convex hull connected by a continuous below sea-level path. A number of examples are shown in Fig. 5c; below sea-level points in the Sermeq Kujalleq ice catchment have an effective position in Disko Bay, points in the Petermann ice catchment have an effective position in Nares Strait, points in Scoresby Sund and the branching

https://doi.org/10.5194/egusphere-2026-6446
Preprint. Discussion started: 16 November 2026
© Author(s) 2026. CC BY 4.0 License.

fjords have an effective position at the mouth of the outer fjord, and numerous other small fjords have effective positions at their respective mouths.

3.2.3 Mapping ("downscaling") CMIP model ocean properties to ISMIP grid

Now, given the regularly-gridded and bias-corrected thermal forcing $\mathrm{TF}_{\mathrm{corrected}}$ (e.g., Fig. 4c), we calculate $z_{\mathrm{reg}}(x_{\mathrm{reg}}, y_{\mathrm{reg}})$, which is the greatest depth at which there is thermal forcing value at grid location $[x_{\mathrm{reg}}, y_{\mathrm{reg}}]$ (Fig. 6a shows an example for the CMIP model CESM2-WACCM). Then, for all below sea-level locations $[x, y]$ on the ISMIP grid, we find the regular grid point, $[\hat{x}_{\mathrm{reg}}(x,y), \hat{y}_{\mathrm{reg}}(x,y)]$, that is closest to $[x_{\mathrm{eff}}(x,y), y_{\mathrm{eff}}(x,y)]$ and that satisfies $z_{\mathrm{reg}}(\hat{x}_{\mathrm{reg}}, \hat{y}_{\mathrm{reg}}) < z_{\mathrm{eff}}(x,y)$. In other words, for each ISMIP grid location that is connected to the ocean, we find the regular grid point that is closest to the corresponding effective position and has properties sufficiently deep. Finally, we define the thermal forcing on the ISMIP grid (Fig. 6c) as

$$\mathrm{TF}_{\mathrm{ISMIP}}(x,y,t) = \mathrm{TF}_{\mathrm{corrected}}(\hat{x}_{\mathrm{reg}}(x,y), \hat{y}_{\mathrm{reg}}(x,y), z_{\mathrm{eff}}(x,y), t) + \lambda_3 \left[z_{\mathrm{eff}}(x,y) - z(x,y)\right] \quad (4)$$

That is, the thermal forcing at a given ISMIP grid point (x, y) is given by the thermal forcing at the effective position and at the effective depth, and then corrected for the fact that the effective depth may differ from the actual depth at (x, y), which would be the glacier grounding line depth if the calving front was located at that point. Any below sea-level regions that are not connected to the ocean (magenta areas in Fig. 5b) are assigned $\mathrm{TF}_{\mathrm{ISMIP}} = 0$.

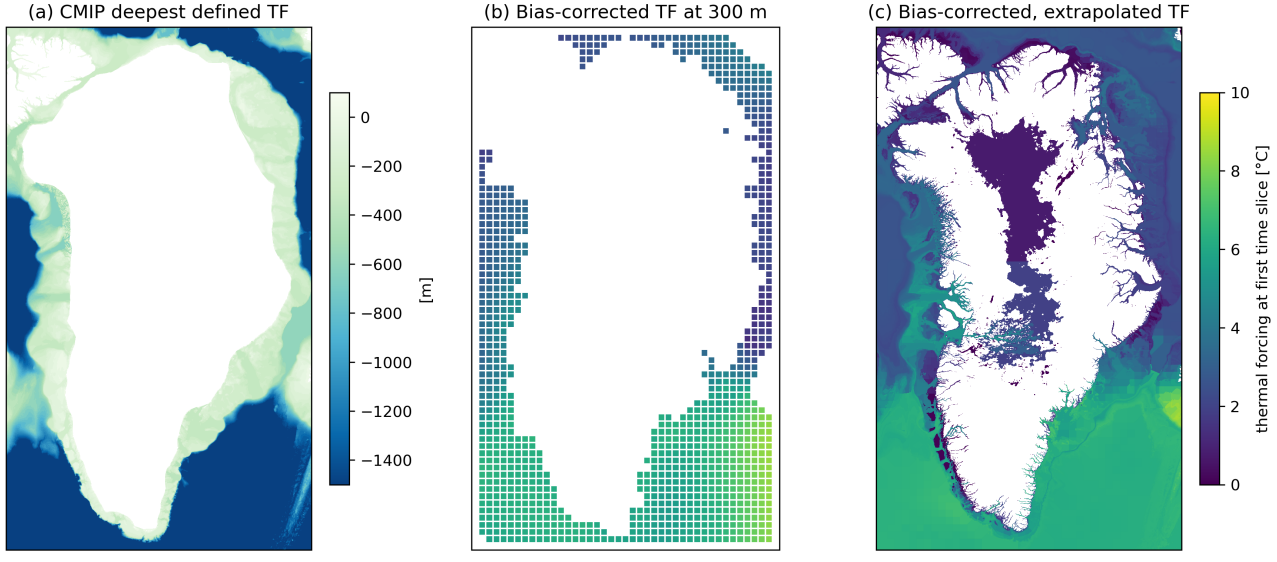


Figure 6. Example of using regular grid output, in this case from CESM2-WACCM, to obtain thermal forcing on the ISMIP grid. (a) Greatest depth of defined thermal forcing for this model (this may differ from Fig. 5a depending on the topography assumed in the CMIP model). (b) Bias-corrected thermal forcing at 300 m depth at a snapshot in time, on the regular grid. (c) Resulting thermal forcing on the ISMIP grid, obtained by extrapolating the properties at effective depth levels such as the snapshot shown in (b) using the algorithm described in the text.

https://doi.org/10.5194/egusphere-2026-6446
Preprint. Discussion started: 16 November 2026
© Author(s) 2026. CC BY 4.0 License.

Although this algorithm is involved to describe, we believe it is the simplest algorithm that has the key attributes we seek. It defines ocean properties at all ISMIP grid points even if the region is not resolved by a CMIP model. The ocean properties come from a physically-reasonable location and account for the potential for bathymetry to block deep, warm waters. The matching of ISMIP grid locations to CMIP model points takes account of the effective depth, which is in turn calculated using BedMachine bathymetry; this means that if a CMIP model has unrealistically shallow bathymetry on the continental shelf, the algorithm looks further offshore to find the deeper water masses that should be able to access the ice sheet margin. The algorithm also has the advantage that the computationally-intensive step – the calculation of the effective positions – does not have to be redone for each individual CMIP model.

4 Use of provided forcings

4.1 Submarine melt rate

4.1.1 Grounded outlet glaciers

In line with making the protocol less prescriptive than in ISMIP6, which had the risk of artificially narrowing the ensemble uncertainties, we are not requiring all models to use a specific submarine melt parameterisation. Models are therefore welcome to use their own parameterisation, but we require that it take into account both subglacial discharge and ocean thermal forcing, given the strong evidence that both play an important role in modulating submarine melting at grounded glaciers (Luckman et al., 2015; Jackson et al., 2022). Existing parameterisations tend to have submarine melt proportional to subglacial discharge raised to a power of around $1/3$ and to ocean thermal forcing raised to a power slightly larger than 1 (e.g., Jackson et al., 2022; Slater and Straneo, 2022).

In practice, a model may choose to use the Rignot et al. (2016) parameterisation (hereafter, the "Rignot parameterisation"), obtained from fitting a functional form to numerical ocean simulations motivated by Store Glacier (Xu et al., 2013). We choose to write the parameterisation out here to avoid confusion with units and definitions

$$m = \lambda (a h q^{\alpha} + b)\,\mathrm{TF}^{\beta} \tag{5}$$

In this form, m is the submarine melt rate in metres per day, $a = 3 \times 10^{-4}$ is a constant, h is the water depth in metres, $q = 86400 \times Q/A$ is the subglacial discharge (Q, m^3/s) normalised by the submerged calving front area (A, m^2), $b = 0.15$ is a constant, TF (°C) is the ocean thermal forcing, $\alpha = 0.39$ and $\beta = 1.18$. The overall scaling parameter, λ, is not present in the original Rignot parameterisation, but we use this to sweep uncertainty in melt rates based on observations (see below).

This parameterisation requires knowledge of the submerged surface area (A) of an outlet glacier, which models could either calculate dynamically or use the provided field for. The provided submerged area field is based on the current ice sheet geometry; therefore, use with ice sheet geometries that differ from that of the present observed extent is an approximation. Note that by this parameterisation, there is the potential for very small submerged areas to lead to very large submarine melt rates. Such a case is likely unphysical (for example if the small submerged area arises due to a glacier becoming close to land-terminating,

https://doi.org/10.5194/egusphere-2026-6446
Preprint. Discussion started: 16 November 2026
© Author(s) 2026. CC BY 4.0 License.



then subglacial discharge will no longer act like a plume and will probably fill the shallow layers of the fjord with cold water). To avoid this, in the provided submerged area field we impose a minimum area of 2 km × 100 m, corresponding to a small marine-terminating glacier. Beyond the continental shelf, we assign a nominal submerged area of 20 km × 400 m, corresponding to a large ice stream, but this is mainly to fill the full grid with some useable value and we do not anticipate any model to use these values (i.e., having a sufficiently advanced ice sheet margin) within the ISMIP simulations. The water depth (h), which should be greater than 0 if the grid cell is ocean, is likely more easily available within an ice sheet model but we provide a reference field on the ISMIP grid in case it is useful.

The Rignot parameterisation can be tuned to match limited available observations using λ. While this form introduces redundancy in the parameters (i.e., we could tune a and b instead), it makes transparent how much the observations depart from the original parameterisation. In addition, we do not feel the limited observations offer sufficient constraint on the individual parameters within the original parameterisation; therefore we leave the original parameterisation unmodified and demonstrate how to tune only the overall magnitude. Observational estimates of submarine melt rate consist of estimates based on ocean heat and salt budgets at Xeitl Sít' (Leconte Glacier), Alaska (Jackson et al., 2022) and at Store Glacier, Eqip Sermia, Kangilerngata Sermia, Sermeq Kujalleq and Sermeq Avannarleq, west Greenland (Rignot et al., 2010; Xu et al., 2013). We also include estimates based on repeat multibeam surveys at Xeitl Sít' (Sutherland et al., 2019; Abib et al., 2023). Each of these studies also provide uncertainties and all of the inputs required to estimate submarine melt via the Rignot parameterisation. We then take a Monte-Carlo approach to generate a confidence interval for λ on the basis of the uncertain observations.

On average, the Rignot parameterisation in its original form (i.e., with $\lambda = 1$) underpredicts the observational estimates of submarine melt rate (Fig. 7a). This is the case despite the fact that the Rignot parameterisation was intended to represent maximum melt rate rather than the frontal area-averaged melt rate that we get from the observations. The obtained distribution for λ is shown in Fig. 7b, with almost all of the probability lying above $\lambda = 1$. From the scatter plot we can see that the Xeitl Sít' budgets estimates are driving λ to higher values while there are notable Xeitl Sít' multibeam points pulling the other way. Budget estimates do not account for iceberg melt between the flux gate and the terminus and so if anything are likely biased high; Jackson et al. (2022) made a rough estimate that this could account for 7% of the melt rate. Meanwhile the multibeam estimates do not account for areas of the front at which significant calving occurred between scans, and since these may also be areas of relatively high melt, there is a suggestion that the multibeam melt rates are likely too low (Sutherland et al., 2019; Abib et al., 2023). Considering these corrections to be beyond the scope of the current effort, we take the data at face value.

Based on this analysis, our recommendation is thus that models using the Rignot parameterisation should adopt $\lambda = \lambda_{50} = 1.64$ (with all other parameters as originally defined), which is the median of the λ distribution (Fig. 7b). To examine uncertainty associated with the melt parameterisation, models could adopt a low value given by the 5th percentile of the distribution ($\lambda_5 = 1.32$) and a high value given by the 95th percentile ($\lambda_{95} = 1.96$). This range represents a confidence interval on λ; that is, assuming that there is a universal underlying value that is equally applicable to all glaciers, it quantifies the uncertainty on λ given the observations.

Models using a different submarine melt rate parameterisation should fix parameters as follows. When $Q = 100$ m^3/s, TF = 5 °C, $h = 200$ m and $A = 8 \times 10^5$ m^2, the Rignot parameterisation with $\lambda = 1.64$ gives a melt rate of 3.31 m/d, and the chosen

https://doi.org/10.5194/egusphere-2026-6446
Preprint. Discussion started: 16 November 2026
© Author(s) 2026. CC BY 4.0 License.

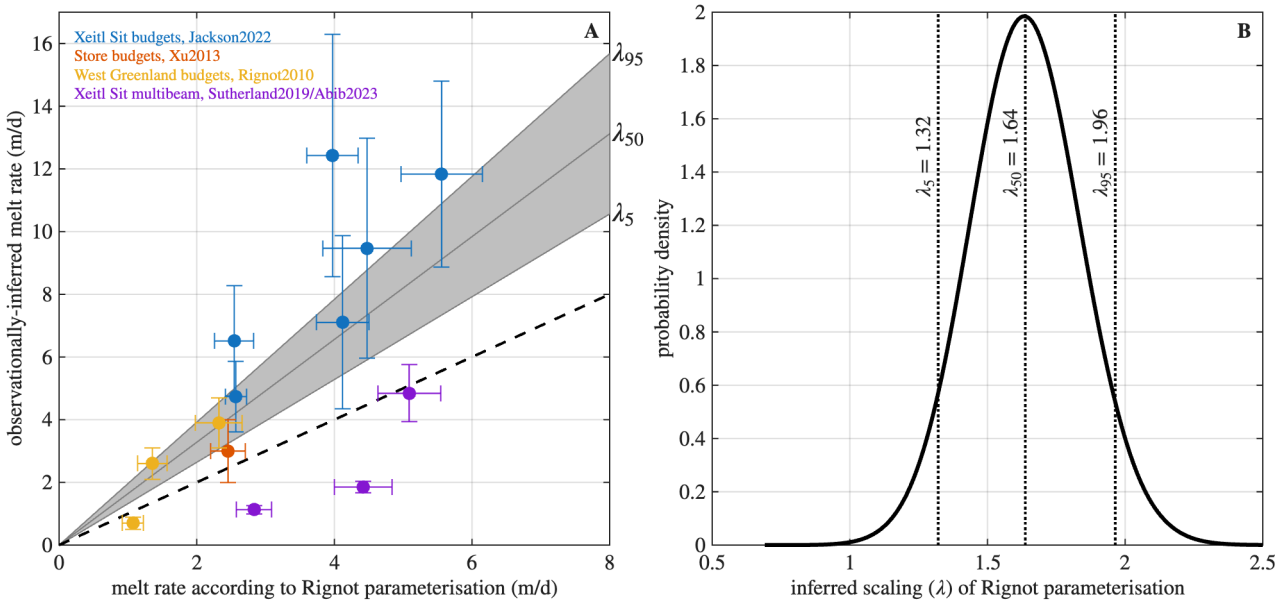


Figure 7. (a) Comparing observationally-inferred melt rates against that predicted by the unscaled Rignot parameterisation (i.e., Eq. 5 with $\lambda = 1$). Marker colours indicate the source of the observation. The black dashed line indicates the 1:1 line; an observational estimate that was perfectly predicted by the parameterisation would sit on this line. The grey shading indicates the 5-95 percentile confidence interval on λ. (b) Probability density for λ, describing confidence on the best-fit relationship between melt from the Rignot parameterisation and observations. The vertical dotted lines illustrate the percentiles selected for ice sheet simulations.

melt rate parameterisation should be tuned to ensure that with these inputs (or at least with this Q and TF), the same melt rate is obtained. The equivalent melt rates for the low and high values of λ are 2.66 m/d and 3.95 m/d, which provide the tuning targets for low and high instances of the chosen melt rate parameterisation.

We anticipate resolution-dependent effects in the representation of submarine melting, as coarser resolutions can aggregate several glacier fronts into a single grid cell, or omit smaller ocean-terminating glaciers. As such, the submarine melt flux in a given geographic area can depend strongly on resolution; further details can be found in Appendix A. We do not advise re-scaling submarine melt rate to try to account for resolution dependence, but raise this as a factor that may help in understanding the ice sheet model ensemble.

4.1.2 Floating ice shelves

For floating ice shelves, we take the same approach of not recommending a particular submarine melt parameterisation, and welcoming ice sheet models to use their preferred approach. Note that due to the different processes happening under a ∼horizontal ice tongue compared to a ∼vertical calving front (Fig. 1), it would not be appropriate to use the same melt parameterisation for both. However, there is evidence that subglacial discharge can elevate submarine melting beneath ice tongues (e.g., Washam et al., 2019). Suitable ice shelf melt parameterisations have been reviewed by Favier et al. (2019) and

https://doi.org/10.5194/egusphere-2026-6446
Preprint. Discussion started: 16 November 2026
© Author(s) 2026. CC BY 4.0 License.

recently employed in the context of Greenland by Verjans et al. (2025). In order to explore uncertainty arising from the parameterisation, we recommend scaling melt rates in the same manner as for grounded glaciers; that is, assume a high scenario that scales the default melt rates by a factor $\lambda_{95}/\lambda_{50} = 1.2$ and a low scenario that scales by a factor $\lambda_5/\lambda_{50} = 0.8$. Some parameterisations require salinity as well as thermal forcing; we therefore provide fields of salinity that are regridded, bias-corrected and extrapolated into fjords in an identical manner as for the thermal forcing. Note, however, that we provide only 3D (time by y by x) fields of ocean properties at the grounding line, rather than full 4D (time by depth by y by x) fields.

4.2 Treatment of calving

As outlined in section 2, we ask ice sheet modeling groups to implement a calving law (or laws) of their own choosing. Our focus group feels that there is not currently sufficient evidence to back a specific calving law and that doing so, or specifying a retreat mask like in ISMIP6, would risk artificially narrowing the ensemble. Therefore, ice sheet models are asked to follow the implementation that they judge to be best in the context of physical process understanding and in the context of their model. Where parameter calibration is necessary, we recommend applying parameters uniformly to the entire ice sheet unless a physical justification exists for regional or local variation. Our hope is that in their implementation, models will have independently moving calving fronts. Note that non-implementation of calving (i.e., relying only on the submarine melt rates generated through our protocol) would mean missing a significant ice sheet mass loss term. We note that there are two different styles of calving parameterisations: those meant to estimate the rate of ice loss due to calving (rate-based parameterisations) and those meant to estimate the position of the glacier terminus (position-based parameterisations). In the conceptualisation in section 2, calving was implicitly defined as rate-based; however, we do not endorse one of these two styles over the other for ISMIP7.

5 Example based on CESM2-WACCM

We illustrate the described protocol with forcings based on the earth system model CESM2-WACCM (Danabasoglu et al., 2020). This is one of the two earth system models chosen for the ISMIP7 core experiments (Nowicki et al., in prep), the other being MRI_ESM2-0 (Yukimoto et al., 2019). We show the historical, ssp126, ssp370 and ssp585 scenarios that are used in the core experiments. As these earth system models are from CMIP6, the historical period covers 1850-2014 and the projection scenarios begin in 2015. The ssp370 scenario extends to 2100, while the ssp126 and ssp585 scenarios extend to 2300. We also show the previously-described OCX forcing, which is derived directly from RACMO and EN4 without the use of an earth system model.

The resulting subglacial discharge is shown in Fig. 8. In the baseline period used for the bias correction (Fig. 8a), large marine-terminating glaciers have subglacial discharge of several hundred m^3/s; the basin with the highest discharge is a currently land-terminating basin in SW Greenland (though if some ice sheet models have a simulation in which the ice sheet is too extended, these values might be used as marine-terminating subglacial discharge). In the intermediate ssp370 scenario, all basins experience an approximate doubling to tripling in subglacial discharge by the end of the century (Fig. 8b), though the

https://doi.org/10.5194/egusphere-2026-6446
Preprint. Discussion started: 16 November 2026
© Author(s) 2026. CC BY 4.0 License.

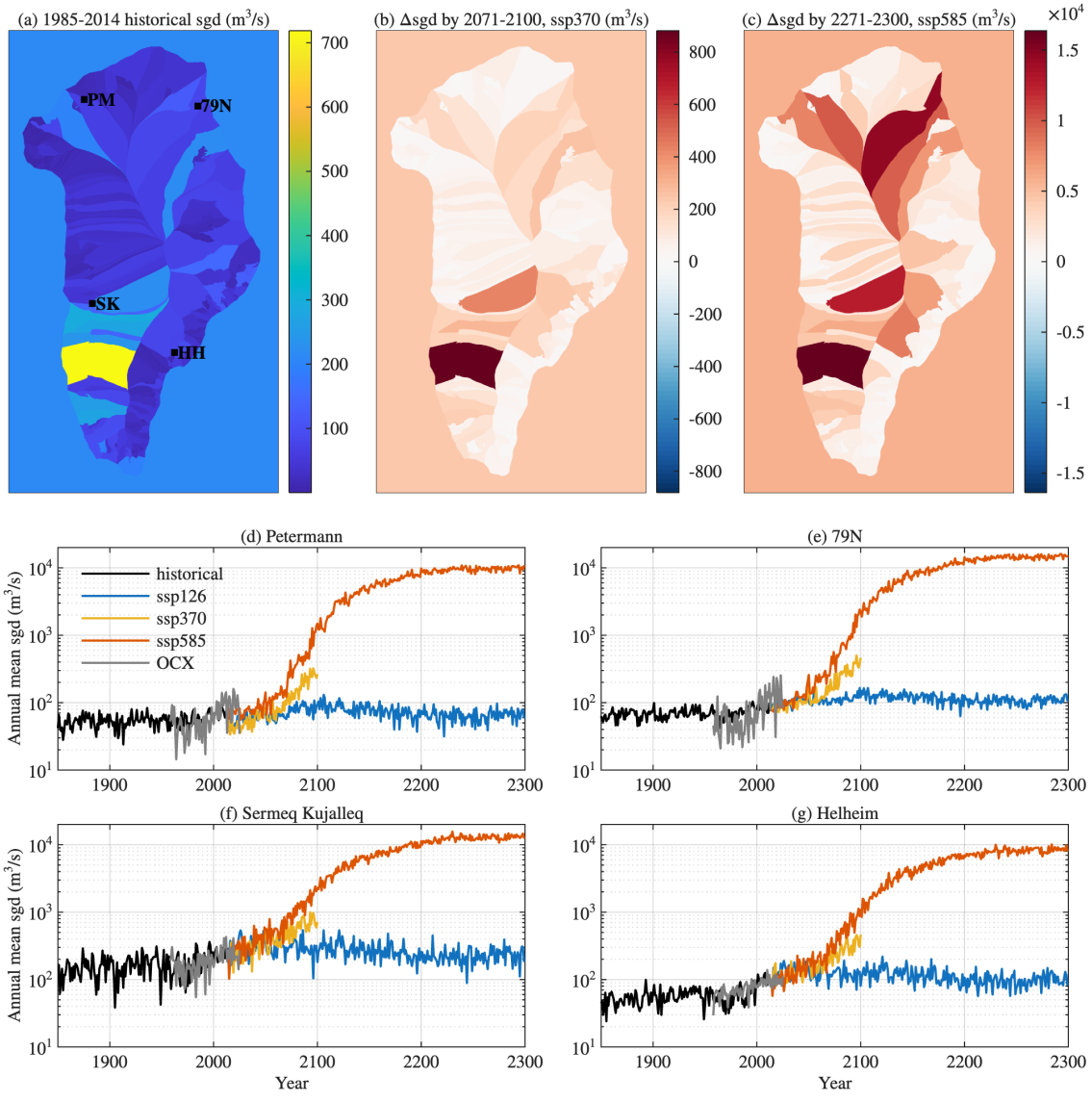


Figure 8. Example subglacial discharge forcing. The historical and projection (ssp126, ssp370, ssp585) scenarios are from CESM2-WACCM. The OCX scenario is based on RACMO. (a) 1985-2014 mean subglacial discharge in the CESM2-WACCM historical simulation. Marked locations are PM: Petermann Glacier; 79N: 79N Glacier; SK: Sermeq Kujalleq; and HH: Helheim Glacier. (b) Difference in subglacial discharge by 2071-2100 (i.e., mean during 2071-2100 minus the mean during 1985-2014) in the ssp370 scenario. (c) Difference in subglacial discharge by 2271-2300 in the ssp585 scenario. Note the different colour scales in (b) and (c). (d)-(g) Time series of annual subglacial discharge extracted for the prominent glaciers having location indicated in (a). Note the log scale on the y-axes and that the climate simulation for ssp370 only extends to 2100.

https://doi.org/10.5194/egusphere-2026-6446
Preprint. Discussion started: 16 November 2026
© Author(s) 2026. CC BY 4.0 License.

colour scale is dominated by the largest basins that have the largest absolute increases. In the high emissions ssp585 scenario and by 2300, there are some extremely large estimates of basin subglacial discharge (Fig. 8c).

Time series for four prominent glaciers are shown in Figs. 8d-g. Although these are extracted from fixed points, whereas in reality we would expect terminus positions to move, these time series will not change provided the terminus remains within the same drainage basin. The CMIP-derived subglacial discharge over the historical period for all glaciers shows interannual and multi-decadal variability, with a trend of increasing subglacial discharge after about 1980. For the ssp126 projection, there is a weakly increasing followed by weakly decreasing subglacial discharge over the projection period, changing the sign of its trend at around 2050 for the southerly glaciers (Sermeq Kujalleq and Helheim), but not until around 2100 for the northerly glaciers. The ssp370 scenario shows significantly increasing subglacial discharge for all glaciers through the 21st century, while the ssp585 scenario shows subglacial discharge increasing drastically before flattening out at very high values post-2200. The climate scenarios diverge significantly after around 2050. Finally, the OCX subglacial discharge represents our best estimate of the subglacial discharge in recent decades, as it is drawn from a regional climate model reanalysis rather than a free running AOGCM, which may not show the same multi-annual variability as observations. The OCX time series show relatively consistent discharge from 1958 to the 1990s, followed by increasing discharge into the 2010s, with particularly large melt years in 2010, 2012 and 2019, and additionally in 2020 and 2023 for the northerly glaciers. Note that (i) we intend all of these statements to be taken qualitatively as we consider a proper analysis of the significance of these trends to be beyond the scope of this manuscript; and (ii) these results are specific to the single earth system model CESM2-WACCM.

The equivalent results for ocean thermal forcing are shown in Fig. 9. The map plots (Fig. 9a-c) show substantially more spatial variability compared to subglacial discharge. This arises from two factors: (i) true spatial variability at the scales resolved by the earth system model (e.g., Fig. 4a); and (ii) apparent spatial variability that actually arises from ocean temperature stratification combined with differing effective depth. Correspondingly, in the historical baseline period, there are clear latitudinal differences in ocean thermal forcing and also bathymetric influences such as warmer waters accessing troughs on the continental shelf (Fig. 9a). By the end of this century in the ssp370 scenario, most of the continental shelf and connected fjords show warming though there is some cooling of shallower areas (Fig. 9b). Near 2300 in the ssp585 scenario there is widespread dramatic warming in all areas (Fig. 9c). The projection time series show some differences by location, with ocean thermal forcing substantially decreasing in the ssp126 scenario at Helheim Glacier (Fig. 9g), remaining relatively constant at Sermeq Kujalleq (Fig. 9f), but increasing at the northerly glaciers (Fig. 9d-e). The southerly glaciers also show little warming in the ssp370 scenario while the northerly glaciers warm significantly. All glaciers eventually warm dramatically in the ssp585 scenario but for the southerly glaciers this does not start until around 2100. Again, these features may be earth system model-specific. The OCX forcing shows slow, gradual warming for the northerly glaciers, and more pronounced warming from the 1980s to 2000s at the southerly glaciers, particularly for Sermeq Kujalleq. Note that we have low confidence in the OCX ocean thermal forcing pre-2000 and for more northerly regions.

Annual mean submarine melt, arising from the subglacial discharge (Fig. 8), ocean thermal forcing (Fig. 9) and the Rignot submarine melt parameterisation (Eq. 5) with $\lambda = 1.64$, is shown in Fig. 10. Note that to calculate the annual mean melt, we first calculate the monthly means using monthly subglacial discharge and ocean thermal forcing, then average over each year.

https://doi.org/10.5194/egusphere-2026-6446
Preprint. Discussion started: 16 November 2026
© Author(s) 2026. CC BY 4.0 License.

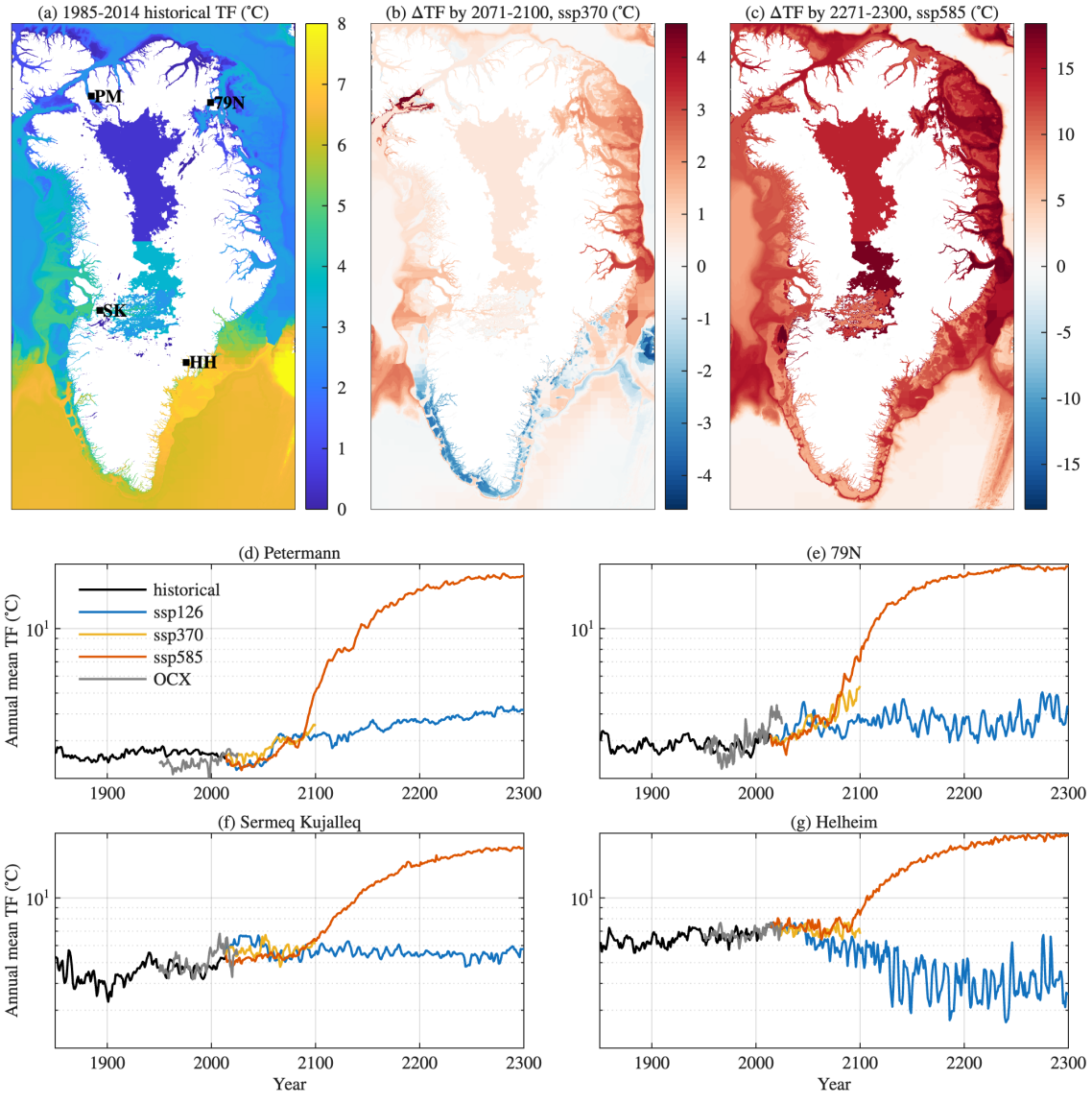


Figure 9. Equivalent of Fig. 8 but for ocean thermal forcing. (a)-(c): Values shown are the ocean thermal forcing that a glacier grounded at that location would experience, i.e., the value at the seafloor accounting for bathymetric blocking of water masses, as described in Section 3.2. Note again the different colour scales on (b) and (c), and the log scale on the y-axes in (d)-(g).

The temporal trends in melt are similar to the constituent parts. It is noticeable that the projection scenarios do not diverge significantly until at least 2050, and possibly later, depending on the location. Towards the end of the ssp585 projection, submarine melt rates reach values far beyond those observed in the present day, so that we can not be certain that the melt parameterisation would still hold. In the OCX melt rates, the northerly glaciers show a gradual increase through the time

https://doi.org/10.5194/egusphere-2026-6446
Preprint. Discussion started: 16 November 2026
© Author(s) 2026. CC BY 4.0 License.

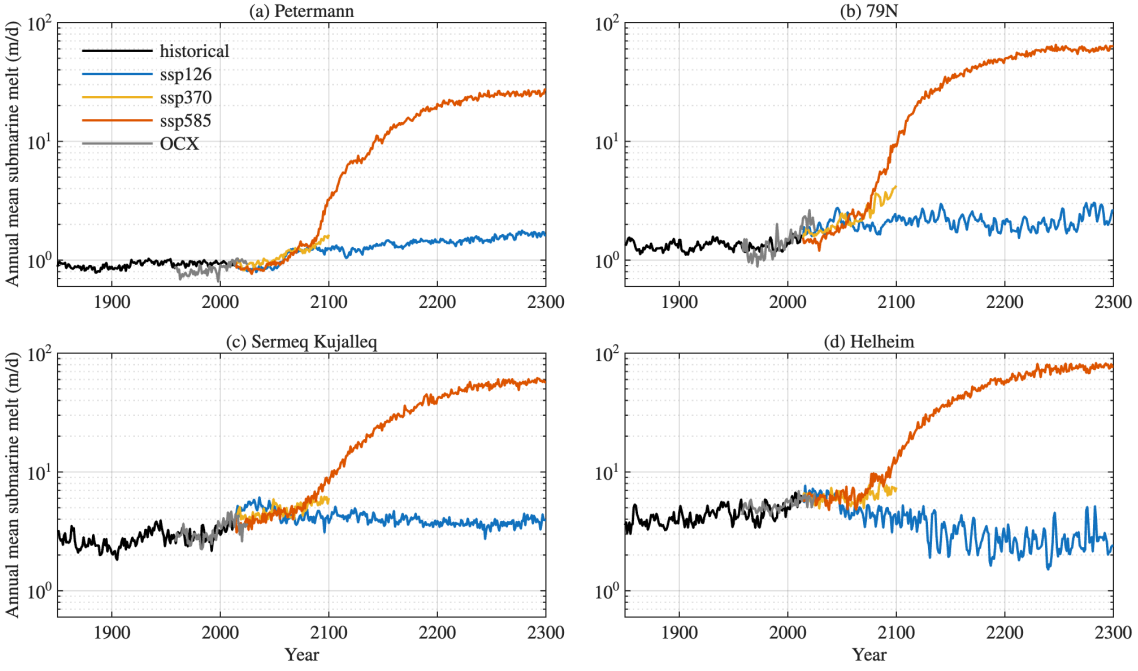


Figure 10. Annual submarine melt for (a) Petermann, (b) 79N, (c) Sermeq Kujalleq and (d) Helheim Glacier, resulting from the subglacial discharge in Fig. 8 and the ocean thermal forcing in Fig. 9 Melt rates are estimated using the Rignot parameterisation (Eq. 5) adjusted with the overall scaling factor $\lambda = 1.64$. Note the log scale on the y-axes.

period (Fig. 10a-b), while the southerly glaciers experience more consistent melt until the late 1990s, followed by an increase into the 2010s (Fig. 10c-d). For the southerly glaciers, these trends are partially captured by the historical simulation.

Lastly, we highlight that although these results plots (Figs. 8-10) display annual means, the provided forcings have monthly temporal resolution, as illustrated in Fig. 11 for the OCX forcing for Sermeq Kujalleq. Since subglacial discharge is highly seasonal, the summer monthly values far exceed the annual values (Fig. 11a vs Fig. 8f). With a glacier effective depth of ∼300 m, the seasonal variability in ocean thermal forcing at Sermeq Kujalleq, inherited from the EN4 product offshore, is much reduced (Fig. 11b), though glaciers with shallower effective depths might have larger seasonal variability in ocean temperature. Submarine melt rates combine the seasonality of the two factors, with interannual variability in the winter submarine melt rate largely determined by the ocean thermal forcing (Fig. 11c). Similar seasonality will be found in the historical and projection CESM2-WACCM forcing, including effects such as a longer “summer” and shorter “winter” in the higher emissions scenarios.

https://doi.org/10.5194/egusphere-2026-6446
Preprint. Discussion started: 16 November 2026
© Author(s) 2026. CC BY 4.0 License.

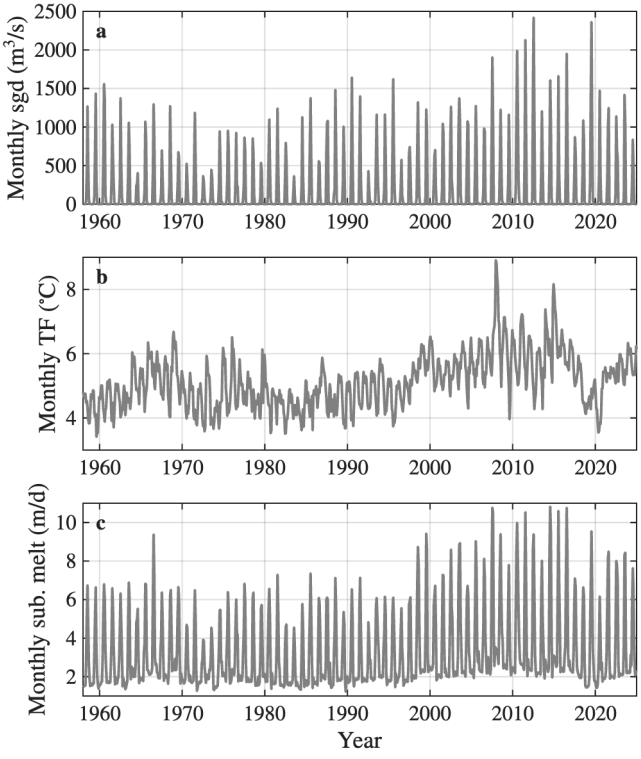


Figure 11. Monthly (a) subglacial discharge, (b) ocean thermal forcing, and (c) submarine melt in the OCX forcing for Sermeq Kujalleq.

6 Discussion

6.1 Differences between ISMIP6 and ISMIP7 Greenland ocean forcing

There are a number of differences between the ISMIP6 Greenland ocean forcing (Slater et al., 2020; Nowicki et al., 2020) and this updated protocol. One overarching difference is that this ISMIP7 protocol is significantly less prescriptive. In ISMIP6, many models ran according to a protocol that directly controlled the position of glacier termini. In the present protocol, the position will be dynamically calculated by ice sheet models, with the implementation of iceberg calving left entirely to the modeling groups. While we introduce a potential submarine melt parameterisation and offer subglacial discharge at the glacier terminus, we also invite deviations from these offerings. Indeed, the only true prescription present within this protocol is the use of the ocean thermal forcing. This philosophical change has the side effect of increasing the decision burden for ice sheet modelers, and will add complexity to the ultimate ensemble analysis. However, given our assessment of uncertainties in the research area, our hope is that a less prescriptive protocol will lead to a more realistic distribution of potential ice sheet futures.

The subglacial discharge basins here follow the ice discharge basins of Mouginot and Rignot (2019) rather than custom hydrologically-calculated basins in ISMIP6. We feel that the practical differences between these basins are limited and the use of a previously-published dataset increases the reproducibility of the dataset, especially as the hydrologically-calculated basins

https://doi.org/10.5194/egusphere-2026-6446
Preprint. Discussion started: 16 November 2026
© Author(s) 2026. CC BY 4.0 License.

need a degree of manual intervention to group sub-basins into a single basin per glacier. In addition, whereas in ISMIP6 the basins were buffered by 3 cells into the ocean from the present-day ice sheet, the basins in ISMIP7 are extended to the full domain to ensure that simulations that have an ice sheet extent much greater than the present day can proceed.

In the ocean thermal forcing, we have implemented a new method for extrapolating ocean properties horizontally into fjords and the ice sheet interior, based on the concept of an "effective position" as well as effective depth (Fig. 5). In ISMIP6, we instead spatially averaged properties over seven basins before extrapolating. The new method avoids artificial ocean property gradients at the basin boundaries and artificial homogeneity within the basins, and samples ocean properties at the location from which they are most likely to come.

The bias correction has also been updated to follow a quantile delta mapping (QDM) method and uses 1985-2014 as the bias correction period. In ISMIP6, both runoff and ocean thermal forcing were bias-corrected only by applying a simple offset to the mean of each CMIP product so that it matched that of a reference product (RACMO or EN4) over the period 1995-2014. Our updated protocol uses QDM to additionally scale the cumulative distribution function of the CMIP ocean thermal forcing, such that the magnitude of variability more closely matches that of the reference product (Cannon et al., 2015). The relative magnitude of seasonal, interannual, and multi-decadal (oscillatory or secular) changes should thus be more consistent with observations in the ISMIP7 forcing products. We now use a reference period extended by 10 years, matching the typical 30-year timescale for computing climatologies, with the expectation that this will better capture decadal-scale variability.

There are also protocol differences that pertain to all of ISMIP rather than just the Greenland ocean forcing. These include the provision of monthly (ISMIP7) rather than annual (ISMIP6) forcing, ensuring that the forcing datasets include seasonality. Previous work has shown that seasonal terminus oscillations can impart a systematic offset in model simulations of outlet glacier mass change on decadal time scales, when compared with simulations that did not include seasonality (Felikson et al., 2022). We also provide CMIP historical and observational-period (OCX) forcings, neither of which was part of ISMIP6.

6.2 OCX forcing

The provision of the OCX forcing aims to allow a better comparison of observed and ice sheet model-simulated mass loss over recent decades. However, there remains significant uncertainty in the OCX forcing. The subglacial discharge is derived from RACMO2.3p2 (Noël et al., 2018); while RACMO2.3p2 compares well with various in-situ climate observations, there can remain significant differences between model-predicted runoff and that observed at stream gauges (Mankoff et al., 2020). In addition, RACMO is just one of many models of surface mass balance and there can be significant inter-model disagreement (Fettweis et al., 2020).

The ocean thermal forcing is estimated using the objective analysis product from EN4 (Good et al., 2013); a gridded product based on ocean profile observations. However, there is high uncertainty associated with this product wherever ocean measurements are spatially or temporally sparse (Ing et al., 2026). This applies to much of Greenland before 2000, and it is really only in the SE and SW after 2000 that the ocean beyond the continental shelf could be said to be reasonably sampled (Verjans et al., 2023). The CW, NW and North of Greenland are particularly poorly sampled. A further source of uncertainty in the OCX ocean thermal forcing arises from the horizontal extrapolation into fjords. Although this is designed to account for the tendency for

https://doi.org/10.5194/egusphere-2026-6446
Preprint. Discussion started: 16 November 2026
© Author(s) 2026. CC BY 4.0 License.

bathymetry to block warm, dense waters, it does not account for any other fjord processes. As such, the ocean thermal forcing in fjords essentially inherits the magnitude and seasonal cycle (e.g. Fig. 11b) of the continental shelf as represented in EN4.

All told, these uncertainties in the OCX forcing, and particularly in the ocean, will complicate any comparison of observed and ice sheet model-simulated mass loss. That is, it will require careful analysis and judgement to know whether a departure of an ice sheet model from the mass loss observations represents a shortcoming with the ice sheet model or instead with the OCX forcing. That said, we expect the temporal variability in the OCX forcing to be more realistic than the equivalent time period in a CMIP AOGCM.

6.3 Implementation of the forcing

We have described the creation and specification of the forcing as precisely as we can, however we anticipate that there will be multiple differences in how ice sheet models implement these forcings. Indeed, we consider inter-model implementation differences to be a feature of the protocol. There will be explicit divergences, such as the choice of submarine melt and calving parameterisations. But there may also be less obvious divergences, for example in how an ice sheet model interpolates from the grid on which the forcing is provided to the ice sheet model native grid. This issue may be particularly acute where a model has a relatively coarse resolution that poorly resolves fjords and individual glaciers. A similar issue may present in the time domain, where models with a short time step are able to apply a seasonal forcing while others essentially apply the annual means. To aid with understanding the ice sheet model ensemble and the behaviour of individual models and simulations, it will be important to document the steps taken when implementing the forcing (see also Appendix B). Ultimately, we believe that allowing different model implementations of the forcing is more effective in mapping out the distribution of potential ice sheet futures than a rigidly prescribed implementation for sampling model structural uncertainty.

6.4 Remaining challenges

With the described protocol, there remain numerous challenges in representing the impact of the ocean on the Greenland Ice Sheet in ice sheet models. The first group of challenges pertains to missing or poorly represented processes. For example, there is still no observationally-validated and community consensus approach to representing Greenland's diverse calving styles in continental-scale ice sheet models (e.g., Benn et al., 2026). The presence of ice melange is thought to significantly modulate calving at the largest glaciers that are most relevant for sea level contribution (e.g., Meng et al., 2025; Deakin et al., 2026), but will likely not be considered by any ice sheet model submission. While widely used parameterisations for submarine melting exist (e.g., Rignot et al., 2016), they remain highly under-constrained by observations (Sutherland et al., 2019; Jackson et al., 2022). Fjord processes beyond the basic bathymetric blocking of dense waters remain unrepresented in the protocol; such processes can influence both the overall magnitude and the seasonal variability of thermal forcing in waters adjacent to the ice sheet, particularly near the fjord surface (Straneo and Cenedese, 2015; Cowton et al., 2023; Wood et al., 2025). Equally, ocean mixing on the continental shelf, internal waves and interaction of currents with the underlying bathymetry (Morrison et al., 2023; Nelson et al., 2025) play a key role in setting the properties of ocean waters at fjord mouths, yet such processes are not resolved by CMIP-scale models.

https://doi.org/10.5194/egusphere-2026-6446
Preprint. Discussion started: 16 November 2026
© Author(s) 2026. CC BY 4.0 License.

For each of these processes, a lack of observations, a lack of process understanding, or the difficulty representing small-scale physics in continental-scale efforts, all to some extent limit our ability to include them in ISMIP7. Further work focusing on (i) process understanding; (ii) the representation of these processes in continental-scale efforts; and (iii) quantifying the potential difference made by these processes to overall sea level contribution, would be highly valuable to efforts such as ISMIP.

A number of inputs to the protocol have been assumed to be fixed but in reality will vary in time. For example, glacial isostatic adjustment (GIA) causes bathymetry to shoal as an ice sheet loses mass, which would change the effective depths. Coastal sea level and the attendant depth of ice-ocean contact is expected to fall by 0.9-2.5 m around Greenland during the 21st century (Lewright et al., 2026). The effect of such change on 21st century Greenland ice sheet dynamics has yet to be directly simulated, but coupled ice-solid earth simulations of Antarctica suggest that bathymetric change may re-stabilize some retreating ice margins, especially in longer-term simulations to 2300 (Adhikari et al., 2014). Similarly, the subglacial discharge basins are assumed fixed but will evolve with ice sheet topography. There is scope in this protocol for ice sheet models to calculate their own, time-evolving, basins (Fig. 2), but otherwise this remains an approximation.

Finally, future efforts could seek to integrate more closely with observations, with particular gains conceivable in the ocean thermal forcing. There are increasing quantities of ocean data from Greenland's fjords (e.g., Roth et al., 2025), and ideally it would be possible to bias-correct the ocean thermal forcing using direct fjord observations rather than EN4. Furthermore, this would increase confidence in the OCX forcing and allow a better comparison of ice sheet models to ice mass loss observations. A barrier to such an effort, however, is the presently disparate nature of Greenland's fjord data (Roth et al., 2025).

7 Conclusions

We have described the protocol for ocean forcing of the Greenland Ice Sheet in ISMIP7. To represent the impact of the ocean, ice sheet modelers are asked to use a calving and submarine melt parameterisation of their choice; we provide the inputs of subglacial discharge and ocean thermal forcing typically needed for these parameterisations. These forcings are derived from CMIP AOGCMs after downscaling, aggregating over basins and bias-correcting (in the case of subglacial discharge), or regridding, bias-correcting and extrapolating into fjords (in the case of ocean thermal forcing). The final forcings are provided on a 1-km regular grid at monthly temporal resolution, for CMIP simulations covering both historical (1850 onwards) and projection (2015 onwards) periods. We also provide an "OCX" forcing, which is our best estimate of how subglacial discharge and ocean thermal forcing have evolved over recent decades, but we note substantial uncertainty in this forcing, particularly in the ocean in northern Greenland and prior to 2000.

The protocol improves on ISMIP6 in several ways, including the higher temporal resolution that resolves seasonality, improved bias correction and improved extrapolation of ocean properties into fjords. Yet, fundamental challenges remain, particularly in the uncertain and observationally under-constrained calving and submarine melt parameterisations, and the difficulty of incorporating continental shelf and fjord processes.

https://doi.org/10.5194/egusphere-2026-6446
Preprint. Discussion started: 16 November 2026
© Author(s) 2026. CC BY 4.0 License.

Code and data availability. All code used in the creation of the forcing datasets is available at https://github.com/ehultee/gris-iceocean-process. CMIP AOGCM outputs are available through Earth System Grid Federation (ESGF) nodes: https://wcrp-cmip.org/cmip-data-access/. EN4 data is available at https://www.metoffice.gov.uk/hadobs/en4/. RACMO2.3p2 data is available at https://www.projects.science.uu.nl/iceclimat data.php and https://zenodo.org/records/19254871. BedMachine Greenland v5 is available at https://nsidc.org/data/idbmg4/versions/5. The output forcing datasets are available at https://www.globus.org/.

Appendix A: Dependence of melt flux on resolution

An initial impression of the dependence of submarine melt flux on model resolution can be obtained without an ice sheet model by using only BedMachine and the forcing fields. To do so, we bilinearly interpolated BedMachine topography, and bilineary and conservatively interpolated the subglacial discharge and ocean thermal forcing, to 1, 2, 4 and 8-km resolutions. For each resolution, we found the pixels having grounded ice, lying below sea level, and in contact with the ocean. Fig. A1 shows the resulting ice-ocean boundary pixels at 1- and 8-km resolution; it is clear that coarser resolution results in fewer "ocean-terminating glaciers".

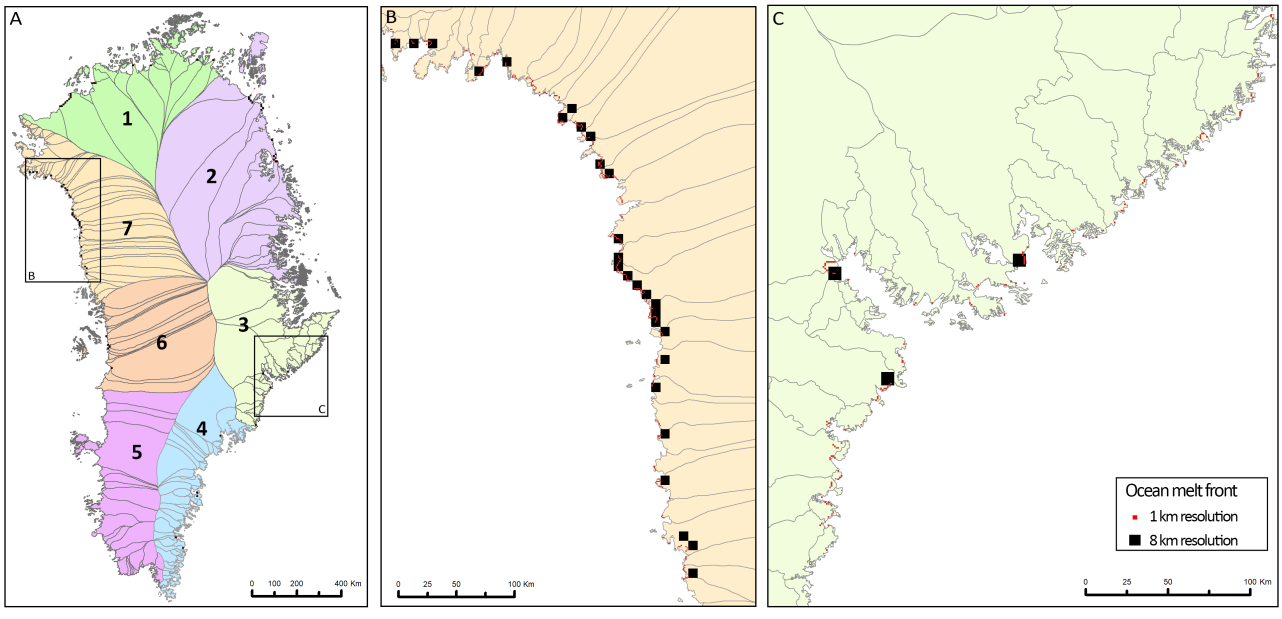


Figure A1. An illustration of the potential impact of resolution on ice-ocean contact area. In the panels, red pixels show ice-ocean boundary cells at 1-km resolution, while black pixels show ice-ocean boundary cells at 8-km resolution. (a) Ice-sheet wide view, (b) zoom to north-west, and (c) zoom to central-east.

Monthly submarine melt rate, for 2016-2025, in the CESM2-WACCM ssp585 scenario, was then calculated following Eq. 5 with $\lambda = 1.64$. For a given resolution, we then averaged over the 10-year time period, and over all ice-ocean pixels in a basin, to obtain a submarine melt rate per basin, given in Table A1. For example, at 1-km resolution, the mean submarine melt rate

https://doi.org/10.5194/egusphere-2026-6446
Preprint. Discussion started: 16 November 2026
© Author(s) 2026. CC BY 4.0 License.

Table A1. Submarine melt rate and flux per ice sheet basin at different resolutions for the CESM2-WACCM ssp585 scenario, 2016-2025. Rates are calculated monthly and then averaged over 2016-2025 and over all pixels in the indicated basin. Fluxes are averaged over 2016-2025 and summed over all pixels in the indicated basin.

	1-km		2-km		4-km		8-km	
Basin	Rate (m/d)	Flux (km^3/yr)	Rate	Flux	Rate	Flux	Rate	Flux
1	0.47	19.95	0.50	15.07	0.63	13.47	0.65	10.25
2	0.37	15.61	0.39	12.23	0.51	10.42	0.42	7.42
3	1.85	18.58	1.84	13.74	2.04	6.71	1.94	1.74
4	3.28	58.57	3.29	31.66	3.14	14.34	3.34	10.49
5	2.28	2.14	2.25	1.35	2.36	1.13	0.00	0.00
6	1.70	18.40	1.78	15.38	1.97	12.56	2.53	12.86
7	0.80	34.81	0.85	31.69	0.82	22.79	0.78	14.95
All	1.11	168.06	1.12	121.11	1.09	81.42	0.97	57.70

over 2016-2025 for all ice-ocean pixels in basin 1 is 0.47 m/d. There is a generally weak dependence of melt rate on resolution, with average melt rate over all basins varying from 0.97 to 1.12 m/d, though there are some basins that are more sensitive - for example basin 5 has no ice-ocean boundary pixels at 8-km resolution.

Finally, we converted the melt rates to a flux by multiplying by the ice-ocean contact area. The melt fluxes show strong sensitivity to resolution, decreasing from a total ice sheet flux of 168 km^3/yr at 1-km resolution to 58 km^3/yr at 8-km resolution (Table A1). This is due principally to the reduced ice-ocean contact area at lower resolution.

https://doi.org/10.5194/egusphere-2026-6446
Preprint. Discussion started: 16 November 2026
© Author(s) 2026. CC BY 4.0 License.

Appendix B: Some practicalities

B1 A note on temporal downsampling

Although the datasets are provided at monthly temporal resolution, some models may prefer to work with annual resolution forcing. To obtain annual values of subglacial discharge (Q) or ocean thermal forcing (TF), we suggest simply averaging the monthly values. There is however a potential pitfall if using a submarine melt parameterisation that is non-linear in Q and/or TF: averaging Q and TF to annual and then calculating submarine melt will give a different value than calculating monthly submarine melt and then taking the annual average. We recommend the latter approach.

B2 A note on spatial resampling to the ice sheet model grid

The subglacial discharge (Q) field is complete with no missing/fill values over the ISMIP grid. The thermal forcing field (TF) has values wherever the 1-km bed topography is at or below sea level. The 1-km bed topography was obtained by downscaling BedMachine v5 values to preserve the mean within a given area. Where the 1-km bed topography is above sea level, the thermal forcing is assigned a value of nan. Thus an interpolation onto the ice sheet model grid will have to deal with these nans - perhaps by taking a conservative average over the non-nan values. It is also possible due to unlucky grid alignment, that a model, say at 8-km resolution, has only nan TF values within a grid cell, in which case looking for the nearest non-nan value seems a sensible approach. We leave this methodological choice open to modellers' best judgement, provided the choice is documented for future reference.

B3 Spatial grid of the provided forcing files (Q, TF, submerged area and water depth)

The forcings are provided on the standard 1-km ISMIP grid, and additionally on a lower resolution 4-km grid. The grid projection is EPSG:3413, i.e., polar stereographic North with standard parallel at 70°N and a central meridian of 45°W. For the 1-km grid, the lower left grid cell center is at (-720000 m, -3450000 m) with nx=1681 and ny=2881 cells in the x- and y-direction at full km positions.

B4 Temporal grid of the provided forcing files (Q and TF)

Monthly temporal resolution, Jan 1850 to Dec 2300, hence nt=5412, formatted as CFtime.DatetimeNoLeap indices. The timestamps are in the middle of the month over which the forcing applies (i.e., the Q and TF for January 1850 are timestamped 1850-01-16). The datasets are split into annual files to keep file size manageable.

B5 Access to the forcing files

The forcing files are freely available on the Globus server hosted at the University at Buffalo (https://app.globus.org), via the ISMIP7 website (https://www.ismip.org), or through Source Cooperative (https://source.coop/ismip) (last accessed: October 2026). On the Globus server, the 1-km resolution data are available at the following paths:

https://doi.org/10.5194/egusphere-2026-6446
Preprint. Discussion started: 16 November 2026
© Author(s) 2026. CC BY 4.0 License.

- TF historical (1850-2014): /ISMIP7/GrIS/<gcm>/historical/ocean-1000m/tf/
- TF projection (2015-2300): /ISMIP7/GrIS/<gcm>/ssp585/ocean-1000m/tf/
- sgd historical (1850-2014): /ISMIP7/GrIS/<gcm>/historical/SDBN1-1000m/sgd/
- sgd projection (2015-2300): /ISMIP7/GrIS/<gcm>/ssp585/SDBN1-1000m/sgd/

Note that throughout this manuscript, subglacial discharge has been referred to as Q, but in the forcing files it is denoted "sgd". We provide three additional files in /ISMIP7/tools/ismip7-gris-ocean-forcing/, which are:

- topg_ismip.nc: 1-km resolution bed topography that was used to do the thermal forcing extrapolation
- basin_submerged_area_ismip.nc: reference calving front submerged area mask that may be required for melt parameterisations, including that of Rignot et al. (2016)
- subglacial_discharge_basins_ismip.nc: mask for the basins used to estimate subglacial discharge.

Author contributions. DS and DF lead the Greenland ocean focus group within ISMIP7 and HG acts as link to the steering committee. DS, LU, DF, HG, MW, TCB and MFdJ contributed to discussion in the design of the protocol. DS, LU and DF wrote the code that undertakes the analysis and did the initial data processing. NS took over the later data processing. MPL contributed the analysis of the sensitivity of melt flux to resolution. DS wrote the manuscript, with input from LU and feedback from all authors.

Competing interests. The authors declare no competing interests.

Acknowledgements. We thank the Heising-Simons Foundation for providing financial support for this study through grant 2025-5727 in support of ISMIP7. DS was supported by the Heising-Simons Foundation grant and by NERC Independent Research Fellowship NE/T011920/1. DF was supported by NASA's Sea-Level Change Team. MPL was supported by the Heising-Simons Foundation grant. HG has received funding from the European Union's Horizon Europe Programme under grant agreement no. 101184939 (SnowPI) and from the Research Council of Norway under projects 350390 (INES2) and 352204 (NorESM4CMIP7). High-performance computing and storage resources were provided by Sigma2 - the National Infrastructure for High Performance Computing and Data Storage in Norway through projects NN5011K, NN8002K, NS5011K and NS8002K. TCB's contributions were supported by the Heising-Simons Foundation.

https://doi.org/10.5194/egusphere-2026-6446
Preprint. Discussion started: 16 November 2026
© Author(s) 2026. CC BY 4.0 License.

References

Abib, N., Sutherland, D. A., Amundson, J. M., Duncan, D., Eidam, E. F., Jackson, R. H., Kienholz, C., Morlighem, M., Motyka, R. J., Nash, J. D., and et al.: Persistent overcut regions dominate the terminus morphology of a rapidly melting tidewater glacier, Annals of Glaciology, 64, 1–12, https://doi.org/10.1017/aog.2023.38, 2023.

Adhikari, S., Ivins, E. R., Larour, E., Seroussi, H., Morlighem, M., and Nowicki, S.: Future Antarctic bed topography and its implications for ice sheet dynamics, Solid Earth, 5, 569–584, https://doi.org/10.5194/se-5-569-2014, 2014.

Barthel, A., Agosta, C., Little, C. M., Hattermann, T., Jourdain, N. C., Goelzer, H., Nowicki, S., Seroussi, H., Straneo, F., and Bracegirdle, T. J.: CMIP5 model selection for ISMIP6 ice sheet model forcing: Greenland and Antarctica, The Cryosphere, 14, 855–879, https://doi.org/10.5194/tc-14-855-2020, 2020.

Benn, D. I., Astrom, J., Zwinger, T., Todd, J., Nick, F. M., Cook, S., Hulton, N. R. J., and Luckman, A.: Melt-under-cutting and buoyancy-driven calving from tidewater glaciers: new insights from discrete element and continuum model simulations, Journal of Glaciology, 63, 691–702, https://doi.org/10.1017/jog.2017.41, 2017.

Benn, D. I., Wheel, I., Christoffersen, P., Åström, J., Cook, S. J., Luckman, A., Nick, F., Hulton, N., Hewitt, I., and Bassis, J.: Calving laws and where to find them, Journal of Glaciology, 72, e22, https://doi.org/10.1017/jog.2026.10128, 2026.

Bondzio, J. H., Seroussi, H., Morlighem, M., Kleiner, T., Rückamp, M., Humbert, A., and Larour, E. Y.: Modelling calving front dynamics using a level-set method: application to Jakobshavn Isbræ, West Greenland, The Cryosphere, 10, 497–510, https://doi.org/10.5194/tc-10-497-2016, 2016.

Cannon, A. J., Sobie, S. R., and Murdock, T. Q.: Bias Correction of GCM Precipitation by Quantile Mapping: How Well Do Methods Preserve Changes in Quantiles and Extremes?, Journal of Climate, 28, 6938 – 6959, https://doi.org/10.1175/JCLI-D-14-00754.1, 2015.

Carroll, D., Sutherland, D. A., Shroyer, E. L., Nash, J. D., Catania, G. A., and Stearns, L. A.: Subglacial discharge-driven renewal of tidewater glacier fjords, Journal of Geophysical Research: Oceans, 122, 6611–6629, https://doi.org/10.1002/2017JC012962, 2017.

Catania, G. A., Stearns, L. A., Moon, T. A., Enderlin, E. M., and Jackson, R. H.: Future Evolution of Greenland's Marine-Terminating Outlet Glaciers, Journal of Geophysical Research: Earth Surface, 125, https://doi.org/10.1029/2018JF004873, 2020.

Cowton, T. R., Slater, D. A., and Inall, M. E.: Subglacial-Discharge Plumes Drive Widespread Subsurface Warming in Northwest Greenland's Fjords, Geophysical Research Letters, 50, e2023GL103 801, https://doi.org/10.1029/2023GL103801, e2023GL103801 2023GL103801, 2023.

Danabasoglu, G., Lamarque, J.-F., Bacmeister, J., Bailey, D. A., DuVivier, A. K., Edwards, J., Emmons, L. K., Fasullo, J., Garcia, R., Gettelman, A., Hannay, C., Holland, M. M., Large, W. G., Lauritzen, P. H., Lawrence, D. M., Lenaerts, J. T. M., Lindsay, K., Lipscomb, W. H., Mills, M. J., Neale, R., Oleson, K. W., Otto-Bliesner, B., Phillips, A. S., Sacks, W., Tilmes, S., van Kampenhout, L., Vertenstein, M., Bertini, A., Dennis, J., Deser, C., Fischer, C., Fox-Kemper, B., Kay, J. E., Kinnison, D., Kushner, P. J., Larson, V. E., Long, M. C., Mickelson, S., Moore, J. K., Nienhouse, E., Polvani, L., Rasch, P. J., and Strand, W. G.: The Community Earth System Model Version 2 (CESM2), Journal of Advances in Modeling Earth Systems, 12, e2019MS001 916, https://doi.org/10.1029/2019MS001916, e2019MS001916 2019MS001916, 2020.

Deakin, K. A., Stokes, C. R., Jamieson, S. S. R., and Carr, J. R.: The Influence of Sea Ice and Ice Mélange on Outlet Glacier Dynamics in the Arctic and Antarctic: Recent Progress and Future Challenges, Reviews of Geophysics, 64, e2025RG000 918, https://doi.org/10.1029/2025RG000918, 2026.

https://doi.org/10.5194/egusphere-2026-6446
Preprint. Discussion started: 16 November 2026
© Author(s) 2026. CC BY 4.0 License.

Edwards, T. L., Nowicki, S., Marzeion, B., Hock, R., Goelzer, H., Seroussi, H., Jourdain, N. C., Slater, D. A., Turner, F. E., Smith, C. J., McKenna, C. M., Simon, E., Abe-Ouchi, A., Gregory, J. M., Larour, E., Lipscomb, W. H., Payne, A. J., Shepherd, A., Agosta, C., Alexander, P., Albrecht, T., Anderson, B., Asay-Davis, X., Aschwanden, A., Barthel, A., Bliss, A., Calov, R., Chambers, C., Champollion, N., Choi, Y., Cullather, R., Cuzzone, J., Dumas, C., Felikson, D., Fettweis, X., Fujita, K., Galton-Fenzi, B. K., Gladstone, R., Golledge, N. R., Greve, R., Hattermann, T., Hoffman, M. J., Humbert, A., Huss, M., Huybrechts, P., Immerzeel, W., Kleiner, T., Kraaijenbrink, P., Le clec'h, S., Lee, V., Leguy, G. R., Little, C. M., Lowry, D. P., Malles, J.-H., Martin, D. F., Maussion, F., Morlighem, M., O'Neill, J. F., Nias, I., Pattyn, F., Pelle, T., Price, S. F., Quiquet, A., Radić, V., Reese, R., Rounce, D. R., Rückamp, M., Sakai, A., Shafer, C., Schlegel, N.-J., Shannon, S., Smith, R. S., Straneo, F., Sun, S., Tarasov, L., Trusel, L. D., Van Breedam, J., van de Wal, R., van den Broeke, M., Winkelmann, R., Zekollari, H., Zhao, C., Zhang, T., and Zwinger, T.: Projected land ice contributions to twenty-first-century sea level rise, Nature, 593, 74–82, https://doi.org/10.1038/s41586-021-03302-y, 2021.

Favier, L., Jourdain, N. C., Jenkins, A., Merino, N., Durand, G., Gagliardini, O., Gillet-Chaulet, F., and Mathiot, P.: Assessment of sub-shelf melting parameterisations using the ocean–ice-sheet coupled model NEMO(v3.6)–Elmer/Ice(v8.3), Geoscientific Model Development, 12, 2255–2283, https://doi.org/10.5194/gmd-12-2255-2019, 2019.

Felikson, D., Nowicki, S., Nias, I., Morlighem, M., and Seroussi, H.: Seasonal Tidewater Glacier Terminus Oscillations Bias Multi-Decadal Projections of Ice Mass Change, Journal of Geophysical Research: Earth Surface, 127, e2021JF006 249, https://doi.org/10.1029/2021JF006249, 2022.

Fettweis, X., Hofer, S., Krebs-Kanzow, U., Amory, C., Aoki, T., Berends, C. J., Born, A., Box, J. E., Delhasse, A., Fujita, K., Gierz, P., Goelzer, H., Hanna, E., Hashimoto, A., Huybrechts, P., Kapsch, M.-L., King, M. D., Kittel, C., Lang, C., Langen, P. L., Lenaerts, J. T. M., Liston, G. E., Lohmann, G., Mernild, S. H., Mikolajewicz, U., Modali, K., Mottram, R. H., Niwano, M., Noël, B., Ryan, J. C., Smith, A., Streffing, J., Tedesco, M., van de Berg, W. J., van den Broeke, M., van de Wal, R. S. W., van Kampenhout, L., Wilton, D., Wouters, B., Ziemen, F., and Zolles, T.: GrSMBMIP: intercomparison of the modelled 1980–2012 surface mass balance over the Greenland Ice Sheet, The Cryosphere, 14, 3935–3958, https://doi.org/10.5194/tc-14-3935-2020, 2020.

Fried, M. J., Catania, G. A., Stearns, L. A., Sutherland, D. A., Bartholomaus, T. C., Shroyer, E., and Nash, J.: Reconciling Drivers of Seasonal Terminus Advance and Retreat at 13 Central West Greenland Tidewater Glaciers, Journal of Geophysical Research: Earth Surface, 123, 1590–1607, https://doi.org/10.1029/2018JF004628, 2018.

Gardner, A. S., Schlegel, N.-J., and Larour, E.: Glacier Energy and Mass Balance (GEMB): a model of firn processes for cryosphere research, Geoscientific Model Development, 16, 2277–2302, https://doi.org/10.5194/gmd-16-2277-2023, 2023.

GEBCO: The GEBCO_2025 Grid - a continuous terrain model for oceans and land at 15 arc-second intervals, https://doi.org/10.5285/37c52e96-24ea-67ce-e063-7086abc05f29, 2025.

Goelzer, H., Nowicki, S., Payne, A., Larour, E., Seroussi, H., Lipscomb, W. H., Gregory, J., Abe-Ouchi, A., Shepherd, A., Simon, E., Agosta, C., Alexander, P., Aschwanden, A., Barthel, A., Calov, R., Chambers, C., Choi, Y., Cuzzone, J., Dumas, C., Edwards, T., Felikson, D., Fettweis, X., Golledge, N. R., Greve, R., Humbert, A., Huybrechts, P., Le clec'h, S., Lee, V., Leguy, G., Little, C., Lowry, D. P., Morlighem, M., Nias, I., Quiquet, A., Rückamp, M., Schlegel, N.-J., Slater, D. A., Smith, R. S., Straneo, F., Tarasov, L., van de Wal, R., and van den Broeke, M.: The future sea-level contribution of the Greenland ice sheet: a multi-model ensemble study of ISMIP6, The Cryosphere, 14, 3071–3096, https://doi.org/10.5194/tc-14-3071-2020, 2020.

Good, S. A., Martin, M. J., and Rayner, N. A.: EN4: Quality controlled ocean temperature and salinity profiles and monthly objective analyses with uncertainty estimates, Journal of Geophysical Research: Oceans, 118, 6704–6716, https://doi.org/10.1002/2013JC009067, 2013.

https://doi.org/10.5194/egusphere-2026-6446
Preprint. Discussion started: 16 November 2026
© Author(s) 2026. CC BY 4.0 License.

Ing, R., Nienow, P., Slater, D., and Medina-Lopez, E.: Investigating the use of Landsat-derived sea surface temperatures as a proxy for changes in ocean forcing of Greenland's marine-terminating outlet glaciers, Journal of Glaciology, 72, e75, https://doi.org/10.1017/jog.2026.10204, 2026.

Jackson, R. H., Motyka, R. J., Amundson, J. M., Abib, N., Sutherland, D. A., Nash, J. D., and Kienholz, C.: The Relationship Between Submarine Melt and Subglacial Discharge From Observations at a Tidewater Glacier, Journal of Geophysical Research: Oceans, 127, e2021JC018 204, https://doi.org/10.1029/2021JC018204, e2021JC018204 2021JC018204, 2022.

Lewright, L., Austermann, J., Piecuch, C. G., Adhikari, S., Davis, J. L., Milne, G. A., and Paxman, G. J. G.: Projections of 21st-century sea-level fall along coastal Greenland, Nature Communications, 17, 353, https://doi.org/10.1038/s41467-025-68182-6, 2026.

Luckman, A., Benn, D. I., Cottier, F., Bevan, S., Nilsen, F., and Inall, M.: Calving rates at tidewater glaciers vary strongly with ocean temperature, Nature Communications, 6, https://doi.org/10.1038/ncomms9566, 2015.

Mankoff, K. D., Noël, B., Fettweis, X., Ahlstrøm, A. P., Colgan, W., Kondo, K., Langley, K., Sugiyama, S., van As, D., and Fausto, R. S.: Greenland liquid water discharge from 1958 through 2019, Earth System Science Data, 12, 2811–2841, https://doi.org/10.5194/essd-12-2811-2020, 2020.

Meng, Y., Lai, C.-Y., Culberg, R., Shahin, M. G., Stearns, L. A., Burton, J. C., and Nissanka, K.: Seasonal changes of mélange thickness coincide with Greenland calving dynamics, Nature Communications, 16, 573, https://doi.org/10.1038/s41467-024-55241-7, 2025.

Morlighem, M.: IceBridge BedMachine Greenland, Version 5, https://doi.org/10.5067/GMEVBWFLWA7X, 2022.

Morlighem, M., Bondzio, J., Seroussi, H., Rignot, E., Larour, E., Humbert, A., and Rebuffi, S.: Modeling of Store Gletscher's calving dynamics, West Greenland, in response to ocean thermal forcing, Geophysical Research Letters, 43, 2659–2666, https://doi.org/10.1002/2016GL067695, 2016.

Morlighem, M., Wood, M., Seroussi, H., Choi, Y., and Rignot, E.: Modeling the response of northwest Greenland to enhanced ocean thermal forcing and subglacial discharge, The Cryosphere, 13, 723–734, https://doi.org/10.5194/tc-13-723-2019, 2019.

Morrison, T. J., Dukhovskoy, D. S., McClean, J. L., Gille, S. T., and Chassignet, E. P.: Mechanisms of Heat Flux Across the Southern Greenland Continental Shelf in 1/10° and 1/12° Ocean/Sea Ice Simulations, Journal of Geophysical Research: Oceans, 128, e2022JC019 021, https://doi.org/10.1029/2022JC019021, 2023.

Mortensen, J., Bendtsen, J., J., M. R., Lennert, K., Truffer, M., M., F., and S., R.: On the seasonal freshwater stratification in the proximity of fast-flowing tidewater outlet glaciers in a sub-Arctic sill fjord, Journal of Geophysical Research: Oceans, 118, 1382–1395, https://doi.org/10.1002/jgrc.20134, 2013.

Motyka, R. J., Dryer, W. P., Amundson, J., Truffer, M., and Fahnestock, M.: Rapid submarine melting driven by subglacial discharge, LeConte Glacier, Alaska, Geophysical Research Letters, 40, 5153–5158, https://doi.org/10.1002/grl.51011, 2013.

Mouginot, J. and Rignot, E.: Glacier catchments/basins for the Greenland Ice Sheet, https://doi.org/10.7280/D1WT11, 2019.

Nelson, M., Straneo, F., Purkey, S. G., Waterhouse, A. F., Fogaren, K. E., and Torres, D. J.: Observations of Water Mass Modification and Cross-Shelf Exchange at Narsaq Trough, Greenland, Journal of Geophysical Research: Oceans, 130, e2024JC022 246, https://doi.org/10.1029/2024JC022246, 2025.

Noël, B., van de Berg, W. J., van Wessem, J. M., van Meijgaard, E., van As, D., Lenaerts, J. T. M., Lhermitte, S., Kuipers Munneke, P., Smeets, C. J. P. P., van Ulft, L. H., van de Wal, R. S. W., and van den Broeke, M. R.: Modelling the climate and surface mass balance of polar ice sheets using RACMO2 – Part 1: Greenland (1958–2016), The Cryosphere, 12, 811–831, https://doi.org/10.5194/tc-12-811-2018, 2018.

https://doi.org/10.5194/egusphere-2026-6446
Preprint. Discussion started: 16 November 2026
© Author(s) 2026. CC BY 4.0 License.

Nowicki, S., Goelzer, H., Seroussi, H., Payne, A. J., Lipscomb, W. H., Abe-Ouchi, A., Agosta, C., Alexander, P., Asay-Davis, X. S., Barthel, A., Bracegirdle, T. J., Cullather, R., Felikson, D., Fettweis, X., Gregory, J. M., Hattermann, T., Jourdain, N. C., Kuipers Munneke, P., Larour, E., Little, C. M., Morlighem, M., Nias, I., Shepherd, A., Simon, E., Slater, D., Smith, R. S., Straneo, F., Trusel, L. D., van den Broeke, M. R., and van de Wal, R.: Experimental protocol for sea level projections from ISMIP6 stand-alone ice sheet models, The Cryosphere, 14, 2331–2368, https://doi.org/10.5194/tc-14-2331-2020, 2020.

Rignot, E., Koppes, M., and Velicogna, I.: Rapid submarine melting of the calving faces of West Greenland glaciers, Nature Geoscience, 3, 187–191, https://doi.org/10.1038/ngeo765, 2010.

Rignot, E., Fenty, I., Xu, Y., Cai, C., and Kemp, C.: Undercutting of marine-terminating glaciers in West Greenland, Geophysical Research Letters, 42, 5909–5917, https://doi.org/10.1002/2015GL064236, 2015.

Rignot, E., Xu, Y., Menemenlis, D., Mouginot, J., Scheuchl, B., Li, X., Morlighem, M., Seroussi, H., den Broeke, M. v., Fenty, I., Cai, C., An, L., and Fleurian, B. d.: Modeling of ocean-induced ice melt rates of five west Greenland glaciers over the past two decades, Geophysical Research Letters, 43, 6374–6382, https://doi.org/10.1002/2016GL068784, 2016.

Robel, A. A., Roe, G. H., and Haseloff, M.: Response of Marine-Terminating Glaciers to Forcing: Time Scales, Sensitivities, Instabilities, and Stochastic Dynamics, Journal of Geophysical Research: Earth Surface, 123, 2205–2227, https://doi.org/10.1029/2018JF004709, 2018.

Roth, A., Straneo, F., Holte, J., Lindeman, M., and Mazloff, M.: A dataset for multidisciplinary applications: thirteen years of ocean observations in Sermilik Fjord, Southeast Greenland, Earth System Science Data, 17, 6025–6048, https://doi.org/10.5194/essd-17-6025-2025, 2025.

Seroussi, H., Nowicki, S., Payne, A. J., Goelzer, H., Lipscomb, W. H., Abe-Ouchi, A., Agosta, C., Albrecht, T., Asay-Davis, X., Barthel, A., Calov, R., Cullather, R., Dumas, C., Galton-Fenzi, B. K., Gladstone, R., Golledge, N. R., Gregory, J. M., Greve, R., Hattermann, T., Hoffman, M. J., Humbert, A., Huybrechts, P., Jourdain, N. C., Kleiner, T., Larour, E., Leguy, G. R., Lowry, D. P., Little, C. M., Morlighem, M., Pattyn, F., Pelle, T., Price, S. F., Quiquet, A., Reese, R., Schlegel, N.-J., Shepherd, A., Simon, E., Smith, R. S., Straneo, F., Sun, S., Trusel, L. D., Van Breedam, J., van de Wal, R. S. W., Winkelmann, R., Zhao, C., Zhang, T., and Zwinger, T.: ISMIP6 Antarctica: a multi-model ensemble of the Antarctic ice sheet evolution over the 21st century, The Cryosphere, 14, 3033–3070, https://doi.org/10.5194/tc-14-3033-2020, 2020.

Shreve, R. L.: Movement of Water in Glaciers, Journal of Glaciology, 11, 205–214, https://doi.org/10.3189/S002214300002219X, 1972.

Slater, D. A. and Straneo, F.: Submarine melting of glaciers in Greenland amplified by atmospheric warming, Nature Geoscience, 15, 794–799, https://doi.org/10.1038/s41561-022-01035-9, 2022.

Slater, D. A., Straneo, F., Felikson, D., Little, C. M., Goelzer, H., Fettweis, X., and Holte, J.: Estimating Greenland tidewater glacier retreat driven by submarine melting, The Cryosphere, 13, 2489–2509, https://doi.org/10.5194/tc-13-2489-2019, 2019.

Slater, D. A., Felikson, D., Straneo, F., Goelzer, H., Little, C. M., Morlighem, M., Fettweis, X., and Nowicki, S.: Twenty-first century ocean forcing of the Greenland ice sheet for modelling of sea level contribution, The Cryosphere, 14, 985–1008, https://doi.org/10.5194/tc-14-985-2020, 2020.

Straneo, F. and Cenedese, C.: The Dynamics of Greenland's Glacial Fjords and Their Role in Climate, Annual Reviews of Marine Science, 7, 89–112, https://doi.org/10.1146/annurev-marine-010213-135133, 2015.

Straneo, F. and Heimbach, P.: North Atlantic warming and the retreat of Greenland's outlet glaciers, Nature, 504, 36–43, https://doi.org/10.1038/nature12854, 2013.

https://doi.org/10.5194/egusphere-2026-6446
Preprint. Discussion started: 16 November 2026
© Author(s) 2026. CC BY 4.0 License.

Sutherland, D. A., Jackson, R. H., Kienholz, C., Amundson, J. M., Dryer, W. P., Duncan, D., Eidam, E. F., Motyka, R. J., and Nash, J. D.: Direct observations of submarine melt and subsurface geometry at a tidewater glacier, Science, 365, 369–374, https://doi.org/10.1126/science.aax3528, 2019.

Todd, J., Christoffersen, P., Zwinger, T., Raback, P., Chauche, N., Benn, D., Luckman, A., Ryan, J., Toberg, N., Slater, D., and Hubbard, A.: A Full-Stokes 3D Calving Model applied to a large Greenlandic Glacier, Journal of Geophysical Research: Earth Surface, 123, 410–432, https://doi.org/10.1002/2017JF004349, 2018.

Verjans, V., Robel, A., Thompson, A. F., and Seroussi, H.: Bias Correction and Statistical Modeling of Variable Oceanic Forcing of Greenland Outlet Glaciers, Journal of Advances in Modeling Earth Systems, 15, e2023MS003 610, https://doi.org/10.1029/2023MS003610, 2023.

Verjans, V., Robel, A. A., Ultee, L., Seroussi, H., Thompson, A. F., Ackermann, L., Choi, Y., and Krebs-Kanzow, U.: The Greenland Ice Sheet Large Ensemble (GrISLENS): simulating the future of Greenland under climate variability, The Cryosphere, 19, 3749–3783, https://doi.org/10.5194/tc-19-3749-2025, 2025.

Washam, P., Nicholls, K. W., Munchow, A., and Padman, L.: Summer surface melt thins Petermann Gletscher Ice Shelf by enhancing channelized basal melt, Journal of Glaciology, 65, 662–674, https://doi.org/10.1017/jog.2019.43, 2019.

Wilson, N., Straneo, F., and Heimbach, P.: Satellite-derived submarine melt rates and mass balance (2011–2015) for Greenland's largest remaining ice tongues, The Cryosphere, 11, 2773–2782, https://doi.org/10.5194/tc-11-2773-2017, 2017.

Winkelmann, R., Dennis, D. P., Donges, J. F., Loriani, S., Klose, A. K., Abrams, J. F., Alvarez-Solas, J., Albrecht, T., Armstrong McKay, D., Bathiany, S., Blasco Navarro, J., Brovkin, V., Burke, E., Danabasoglu, G., Donner, R. V., Drüke, M., Georgievski, G., Goelzer, H., Harper, A. B., Hegerl, G., Hirota, M., Hu, A., Jackson, L. C., Jones, C., Kim, H., Koenigk, T., Lawrence, P., Lenton, T. M., Liddy, H., Licón-Saláiz, J., Menthon, M., Montoya, M., Nitzbon, J., Nowicki, S., Otto-Bliesner, B., Pausata, F., Rahmstorf, S., Ramin, K., Robinson, A., Rockström, J., Romanou, A., Sakschewski, B., Schädel, C., Sherwood, S., Smith, R. S., Steinert, N. J., Swingedouw, D., Willeit, M., Weijer, W., Wood, R., Wyser, K., and Yang, S.: The Tipping Points Modelling Intercomparison Project (TIPMIP): Assessing tipping point risks in the Earth system, EGUsphere, 2025, 1–52, https://doi.org/10.5194/egusphere-2025-1899, 2025.

Wood, M., Rignot, E., Fenty, I., An, L., Bjørk, A., van den Broeke, M., Cai, C., Kane, E., Menemenlis, D., Millan, R., Morlighem, M., Mouginot, J., Noël, B., Scheuchl, B., Velicogna, I., Willis, J. K., and Zhang, H.: Ocean forcing drives glacier retreat in Greenland, Science Advances, 7, eaba7282, https://doi.org/10.1126/sciadv.aba7282, 2021.

Wood, M., Fenty, I., Khazendar, A., and Willis, J. K.: Feedbacks Between Fjord Circulation, Mélange Melt, and the Subglacial Discharge Plume at Kangerlussuaq Glacier, East Greenland, Journal of Geophysical Research: Oceans, 130, e2024JC021 639, https://doi.org/10.1029/2024JC021639, 2025.

Xu, Y., Rignot, E., Fenty, I., Menemenlis, D., and Flexas, M. M.: Subaqueous melting of Store Glacier, West Greenland from three-dimensional, high-resolution numerical modeling and ocean observations, Geophysical Research Letters, 40, 4648–4653, https://doi.org/10.1002/grl.50825, 2013.

Yukimoto, S., Kawai, H., Koshiro, T., Oshima, N., Yoshida, K., Urakawa, S., Tsujino, H., Deushi, M., Tanaka, T., Hosaka, M., Yabu, S., Yoshimura, H., Shindo, E., Mizuta, R., Obata, A., Adachi, Y., and Ishii, M.: The Meteorological Research Institute Earth System Model Version 2.0, MRI-ESM2.0: Description and Basic Evaluation of the Physical Component, Journal of the Meteorological Society of Japan. Ser. II, 97, 931–965, https://doi.org/10.2151/jmsj.2019-051, 2019.